

INFORMATION TO USERS

This material was produced from a microfilm copy of the original document. While the most advanced technological means to photograph and reproduce this document have been used, the quality is heavily dependent upon the quality of the original submitted.

The following explanation of techniques is provided to help you understand markings or patterns which may appear on this reproduction.

1. The sign or "target" for pages apparently lacking from the document photographed is "Missing Page(s)". If it was possible to obtain the missing page(s) or section, they are spliced into the film along with adjacent pages. This may have necessitated cutting thru an image and duplicating adjacent pages to insure you complete continuity.
2. When an image on the film is obliterated with a large round black mark, it is an indication that the photographer suspected that the copy may have moved during exposure and thus cause a blurred image. You will find a good image of the page in the adjacent frame.
3. When a map, drawing or chart, etc., was part of the material being photographed the photographer followed a definite method in "sectioning" the material. It is customary to begin photoing at the upper left hand corner of a large sheet and to continue photoing from left to right in equal sections with a small overlap. If necessary, sectioning is continued again — beginning below the first row and continuing on until complete.
4. The majority of users indicate that the textual content is of greatest value, however, a somewhat higher quality reproduction could be made from "photographs" if essential to the understanding of the dissertation. Silver prints of "photographs" may be ordered at additional charge by writing the Order Department, giving the catalog number, title, author and specific pages you wish reproduced.
5. PLEASE NOTE: Some pages may have indistinct print. Filmed as received.

University Microfilms International

300 North Zeeb Road
Ann Arbor, Michigan 48106 USA
St. John's Road, Tyler's Green
High Wycombe, Bucks, England HP10 8HR

77-21,408

SPEARS, David Paul, 1941-
SATELLITE STRUCTURE IN THE PHOTOELECTRON
SPECTRA OF RARE GASES, SOME SIMPLE GASEOUS
MOLECULES, AND ALKALI METAL HALIDES.

The University of Oklahoma,
Ph.D., 1973
Physics, atomic

Xerox University Microfilms, Ann Arbor, Michigan 48106

THE UNIVERSITY OF OKLAHOMA
GRADUATE COLLEGE

SATELLITE STRUCTURE IN THE PHOTOELECTRON SPECTRA
OF RARE GASES, SOME SIMPLE GASEOUS MOLECULES,
AND ALKALI METAL HALIDES

A Dissertation
submitted to the Graduate Faculty
in partial fulfillment of the requirements for the
degree of
Doctor of Philosophy

by
David Paul Spears
Norman, Oklahoma

1973

SATELLITE STRUCTURE IN THE PHOTOELECTRON SPECTRA OF RARE GASES,
SOME SIMPLE GASEOUS MOLECULES, AND ALKALI METAL HALIDES

APPROVED BY

W. S. Fisher

S. E. Beebe, Jr.

Jimmie Sharf

Thomas Carlin

Robert S. Mulliken

DISSERTATION COMMITTEE

ACKNOWLEDGEMENT

The author wishes to thank Dr. H. J. Fischbeck for his encouragement and advice during this work. He also wishes to express his gratitude to Dr. T. A. Carlson for his guidance and patience through to the completion of this research. The assistance of, and consultation with Drs. M. O. Krause and O. Keski-Rahkonen is also appreciated. The author would also like to thank Dr. L. D. Hulet for his help.

A special thanks to Frank H. Ward, who kept putting the pieces back together, H. L. (Barney) Barnwell, who was able to find all of those lost electrons, to M. F. Phillips, who kept replacing destroyed equipment, and to B. S. Dunlap for the excellent drawings.

The author wishes to express his gratitude to Lynda Hawkins, Joan Cotter, Althea Tate and Lee Pogue for their typing and making it all a little easier.

The author wishes to thank the Physics Division of the Oak Ridge National Laboratory* for its hospitality and to the Oak Ridge Associated University for making the research possible.

Finally, a tack skall du ha to his wife Ba who was able to survive this insane trip through purgatory.

*Operated by Union Carbide Corporation for the Energy Research and Development Administration.

LIST OF TABLES

TABLE	PAGE
I. Sample Purity	18
II. Excitation Energy and Intensities of Satellite Structure in the Photoionization of Core Shells of the Rare Gases . .	39
III. Excitation Energy and Intensities of Satellite Structure in the Photoionization of Outer Shells of the Rare Gases . .	52
IV. Analysis of Satellite Structure in the Photoelectron Spectra of the s and p Shells of the Alkali Metal Ions	53
V. Analysis of Satellite Structure in the Photoelectron Spectra of the Inner Orbitals of Nitric Oxide	71
VI. Analysis of Satellite Structure in the Photoelectron Spectra of the Inner Orbitals of Nitrous Oxide	72
VII. Analysis of Satellite Structure in the Photoelectron Spectra of the Inner Orbitals of Water	73
VIII. Atomic Contributions to Atomic Orbitals for N_2	82
IX. Analysis of Valence Shell Photoelectron Spectra of N_2	86

LIST OF FIGURES

FIGURE	PAGE
1. Schematic diagram of photoelectron spectrometer and associated equipment	8
2. Spherical sector plates.	9
3. Schematic diagram of target chamber used for gas studies and the electron gun used for inelastic collision studies	10
4. X-ray tube	12
5. Block diagram of electron spectrometer	15
6. Sample holder and transfer chamber for solids	20
7. Photoelectron spectra of Ar2s, Ar2p and associated satellite structures using $M_gK\alpha$ x-rays	34
8. Photoelectron spectra of Kr3p, Kr3d and associated satellite structures using $M_gK\alpha$ x-rays	35
9. Photoelectron spectra of Xe3d, Xe4d and associated satellite structures using $M_gK\alpha$ x-rays respectively for irradiation	36
10. Photoelectron spectra of Cs4d in CsCl and associated satellite structure using $M_gK\alpha$ x-rays	37
11. Photoelectron spectra of I3d, I4d and CH_3I and their associated satellite structures using $M_gK\alpha$ x-rays . . .	38
12. Photoelectron spectrum of Ar3s and associated satellite structure using $M_gK\alpha$ x-rays	46

FIGURE	PAGE
13. Photoelectron spectra of Ar3p, Ar3s and their associated satellite lines using the $ZrM\zeta$ x-ray	47
14. Photoelectron spectrum of Ar3s showing associated satellite lines of the Ar3s and Ar3p using the $ZrM\zeta$ x-ray	48
15. Photoelectron spectrum of Kr4s and associated satellite lines using $MgK\alpha$ x-rays	49
16. Photoelectron spectra of Xe5s and associated satellite lines using $MgK\alpha$ x-rays	50
17. Photoelectron spectra of Xe5p, Xe5s and their associated satellite lines using $MgK\alpha$ x-rays	51
18. Photoelectron spectra of outer shells of Kr and Rb^+ in RbCl and their associated satellite lines using $MgK\alpha$ x-rays	56
19. Photoelectron spectrum of valence shells of CsCl showing satellite structure associated with the Cs5s using $MgK\alpha$ x-rays	57
20. N1s photoelectron spectrum of nitric oxide and associated satellite structure using $MgK\alpha$ x-rays	67
21. O1s photoelectron spectrum of nitric oxide and associated satellite structure using $MgK\alpha$ x-rays	68
22. N1s photoelectron spectrum of nitrous oxide and associated satellite structure using $MgK\alpha$ x-rays	69
23. O1s photoelectron spectra of nitrous oxide and water showing their respective satellite structure using $MgK\alpha$ x-rays	70

FIGURE	PAGE
24. Photoelectron spectrum of valence shells of N_2 using $ZrM\zeta$ x-rays	87

TABLE OF CONTENTS

CHAPTER	PAGE
I. INTRODUCTION	1
History	1
Configuration-Interaction	3
Electron Shake-Up	3
Research Topic	4
II. EXPERIMENTAL	7
Electron Spectrometer	7
X-ray Tube	11
Spectrometer Slits and Plates	14
Experimental Procedure	17
Sources of Error	19
III. THEORY	22
A. Sudden Approximation	22
B. Configuration-Interaction	26
C. SCF Hartree-Fock	
IV. Rare Gases and Alkali Metal Ions	33
Inner Shells of the Rare Gases	33
Satellite Lines in the X-Ray Photoelectron Spectra of the Outer Shells	45
Alkali Metals	62
V. SATELLITE STRUCTURE IN MOLECULES	66
Photoionization in Core Shells	66
Nitric Oxide	75
Nitrous Oxide	79

CHAPTER	PAGE
Photoelectron Spectra of Valence Shells	85
Summary	88
LIST OF REFERENCES	90

To Scul Sistah of Puddle View.

SATELLITE STRUCTURE IN THE PHOTOELECTRON SPECTRA OF RARE GASES,
SOME SIMPLE GASEOUS MOLECULES, AND ALKALI METAL HALIDES

By: David P. Spears

Major Professor: H.J. Fischbeck

A study is made of the satellite structure in the photoelectron spectra of Ar, Kr and Xe. This includes a study of the photoelectron spectra of both the inner and outer shells using Al K_{α} , Mg K_{α} , and, in some instances, Zr M_{ζ} x-rays for irradiation of the atoms. The satellite structure observed in the photoelectron spectra of the inner shells is consistent with the sudden approximation. The satellite structure in the outer shell photoelectron spectra of Ar, Kr and Xe are found to be due mainly to configuration mixing. The satellite structure associated with the outer shell photoelectron spectra of the alkali and metal ions are compared with those of the isoelectronic rare gases.

Also, a study is made of the inner orbitals of nitric oxide, nitrous oxide and water using Mg K_{α} x-rays for irradiation. The energy separations of the satellite lines are compared with monopole-allowed states of the neutral molecule and of an isoelectronic ion. Finally, the photoelectron spectrum of the valence shells of nitrogen is studied using a Zr M_{ζ} characteristic x-ray as a photon source.

CHAPTER I

INTRODUCTION

History

Electron spectroscopy is an experimental technique in which the kinetic energy of an ejected electron is measured. The field can be broken down into several different subgroups which depend on the excitation process and origin of the ejected electron. They are electron impact electron spectroscopy, beta-ray spectroscopy, Auger spectroscopy, Penning ionization spectroscopy (a study of ejected electrons produced by bombarding material with excited atoms or molecules) and, the topic of this study, photoelectron spectroscopy.

Photoelectron spectroscopy was introduced as an experimental tool in the first part of this century. Innes⁽¹⁾ was one of the first to analyze the kinetic energies of the "cathodic" particles using a magnetic field. He used soft x-rays for the photon source and photographic plates for his detection system. In 1914 Robinson and Rawlinson⁽²⁾ repeated Innes' experiment in greater detail.

Little was done in the field for several decades until 1951 when Steinhardt and Serfass⁽³⁾ pointed out the possibility of using photoelectron spectroscopy (PES) as a method for chemical analysis. However, this work was not followed up with an extensive research effort.

About this same time Siegbahn and his group at Uppsala, Sweden initiated a program in high resolution electron spectroscopy. Siegbahn, whose previous experience had been in β -ray spectroscopy, was able to design and build a high resolution magnetic spectrometer.⁽⁴⁾ Their first measurement of electron binding energies was published in 1957.⁽⁵⁾

The basic relation of PES is given by

$$E_{\text{kin}} = h\nu - E_b \quad (1)$$

where E_{kin} is the kinetic energy of the ejected photoelectron, $h\nu$ is the photon energy and E_b is the binding energy. This is the "normal" photoelectron process. E_b can be defined as

$$E_b = E_f - E_i \quad (2)$$

where E_i and E_f are the total energies of the initial and final states of the neutral atom and the resultant ion. In the normal photoionization process there is only one final state, E_f , of the ion. For monoenergetic photons the electrons ejected from each subshell of the atom should have one specific kinetic energy, i.e. when E_f gives the energy of the ground state of the ion. However, in some instances of photoionization there is a possibility of multiple ionization or excitation where one or more electrons will be ejected into the continuum or move to different orbitals, leaving the ion in an excited configuration. When this happens the energy of this final excited state is E_f^* . In the case of excitation the energy of the ejected photoelectron will be given by

$$E_{\text{kin}} = h\nu - (E_f^* - E_i) \quad (3)$$

The energy of the photoelectron will differ from the energy of the normal photoelectron by the amount $E_f^* - E_f$. In this thesis the processes that lead to excited configurations are to be studied. This will include (1) configuration-interaction and (2) electron shake-up.

Configuration-Interaction

Separate single electron wave functions do not adequately describe a many-body system. It is necessary in order to describe such a situation to consider an admixture of excited unoccupied orbitals, i.e. configuration mixing. These excited orbitals, or other possible final states, must follow specific selection rules. They all must be of the same parity and have the same total angular momentum, and where Russel-Saunders coupling is valid, the same total L and S .⁽⁶⁾

Electron Shake-up

Upon photoionization of an electron from an innershell the outer electrons feel a sudden change in potential. This sudden change can cause the outer electrons to be excited to another orbital, "shake-up," or to be ejected into the continuum, "shake-off." The shake-up, shake-off phenomena fall within the framework of the sudden approximation⁽⁷⁾ and therefore the transitions are restricted by the monopole selection rules

$$\Delta J = \Delta L = \Delta S = 0 \quad .$$

This means that the allowed transitions for an electron in level $n\ell j$ can be excited to the orbital $n'\ell j$, i.e. only the principal quantum number changes for a monopole transition.

Research Topic

If either shake-up or configuration-interaction occurs following ionization, it will be evident in the photoelectron spectrum. These excited states will appear as small satellite peaks with higher binding energies than the normal photoelectron line.

Previous studies of satellite lines in the photoelectron spectra of He^(8,9,10,11) and Ne^(10,12,13,14,15) have been made. Previously, there has been preliminary study of the satellite lines seen in the photoelectron spectrum of Ar.⁽¹⁰⁾ Wuilleumier and Krause^(11,14) performed an angular and energy analysis of the photoelectron spectra of He and Ne. The satellite lines in both the He and Ne photoelectron spectra were found to be, for the most part, a result of monopole transitions. However, it has been observed for photoionization in the outer shells⁽⁸⁾ that the theoretical probability of multiple ionization using single-electron wave function was lower than the measured value. It was found, using correlated wave functions for the ground state of He instead of single electron wave functions, that there was excellent agreement with the experimental values.⁽²¹⁾

Wertheim and Rosencwaig⁽¹⁶⁾ have conducted studies of the satellite lines in the photoelectron spectra of the valence shells of the alkali metal ions. They attributed the intense satellite lines to configuration-interaction.

Also, there have been studies of the satellite lines in the photoelectron spectra of several simple gaseous molecules.^(10,13,15) The spectra of the valence shells can be compared with optical data, whereas for photoionization of inner shells the satellite structure has been explained

by comparing the energies with monopole allowed transitions of the neutral molecule⁽¹⁷⁾ and an isoelectronic molecule.⁽¹⁰⁾ The monopole selection rules for a molecule are

$$\Delta J = \Delta M = \Delta L = \Delta \Sigma = 0 \quad .$$

Thus, the photoelectron spectrum reveals the nature of excitation processes by the presence of satellite structure. To better understand atomic and molecular systems and to get some insight into the excitation mechanism involved in the transitions to excited states, a study of the rare gases Ar, Kr and Xe, the alkali metal ions, and several simple molecules was carried out. The study of the rare gases included a study of the satellite lines in the photoelectron spectra of both the inner and outer shells. The satellite structure in the photoelectron spectra of the inner shells are examined as a function of core vacancy. Comparing the energies of the satellite lines with calculation by Nestor* the energy separations of the satellite peaks were shown to be consistent with the assumption that they could be explained by invoking the sudden approximation.

The satellite lines in the photoelectron spectra of the outer shells of the rare gases are compared with optical data.^(18, 19, 20) In the case of argon and krypton excellent agreement with optical data was found and the proper configuration assignments are made. For argon and krypton configuration-interaction was found to be more important than electron shake up. For xenon definite configuration assignments could not be made.

*Cf. Table II (g).

The alkali metal ions are isoelectronic with the rare gases, and one might expect their satellite structure to be similar. The photoelectron spectra of the valence shells of the alkali halides NaCl, KCl, KBr, RbCl and CsCl were run and the satellite structures are compared with those of the rare gases.

In the final part of the thesis the satellite lines in the spectra of NO, N₂O, H₂O and N₂ are discussed. The satellite structure associated with the photoelectron spectra of the inner shells of NO, N₂O and H₂O are studied using the MgK α x-rays for irradiation.

The data are analyzed by comparing them with the monopole excited energy levels of the neutral molecule and with monopole allowed excitation of an isoelectronic ion. The spectrum of the outer molecular orbitals of N₂ is taken using a Zr M ζ 151.4 eV x-ray as the photon source. The N₂ spectrum is compared with a spectrum taken using MgK α ⁽¹³⁾ and AlK α ⁽¹⁵⁾ x-rays as the photon source.

CHAPTER II

EXPERIMENTAL

Electron Spectrometer

The double focusing electron spectrometer used in this experiment is located in the Physics Division of the Oak Ridge National Laboratory. The spectrometer was built by the ORNL machine shop and is described elsewhere. ⁽²²⁾ The main part of the spectrometer is shown in Figure 1 illustrating the source chamber used for the irradiation of solid samples; the two spherical sector plates which, by placing equal positive and negative potentials on the inner and outer plates respectively, generate an electric field used for the kinetic energy analysis of the electrons; and the electron detector. The shape of the two electrostatic plates and the rods used to correct for any fringe effects on the electric field are shown in Figure 2. In Figure 3 the target chamber used for gases and the electron gun used for the inelastic collision studies are illustrated.

The basic procedure of the experiment is to irradiate the sample in the target chamber with soft x-rays and to analyze the ejected photoelectrons according to their kinetic energy. The photoelectrons pass through the spectrometer entrance slits, and are then focused by the electric field between the spectrometer plates, so that those electrons

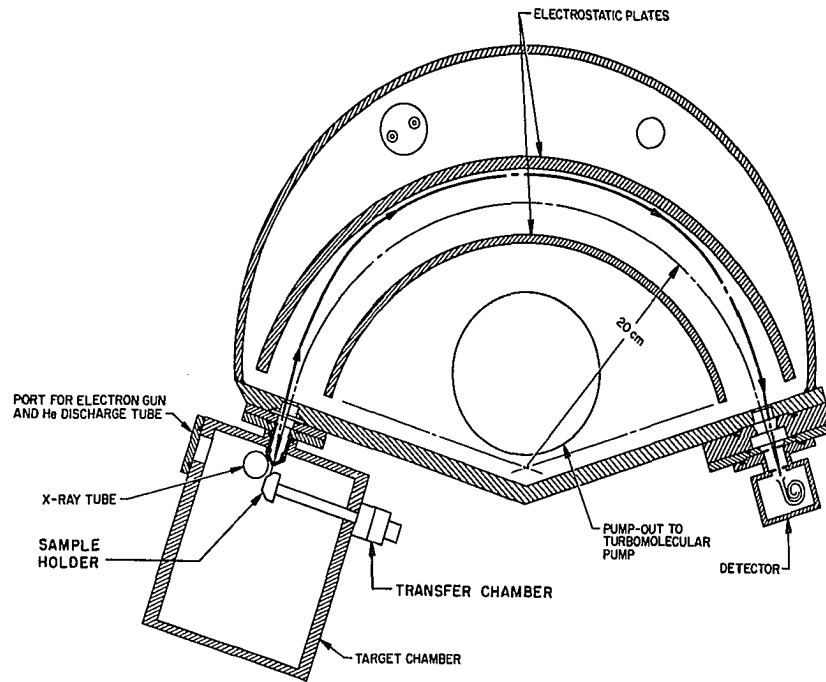


Figure 1. Schematic diagram of photoelectron spectrometer and associated equipment.

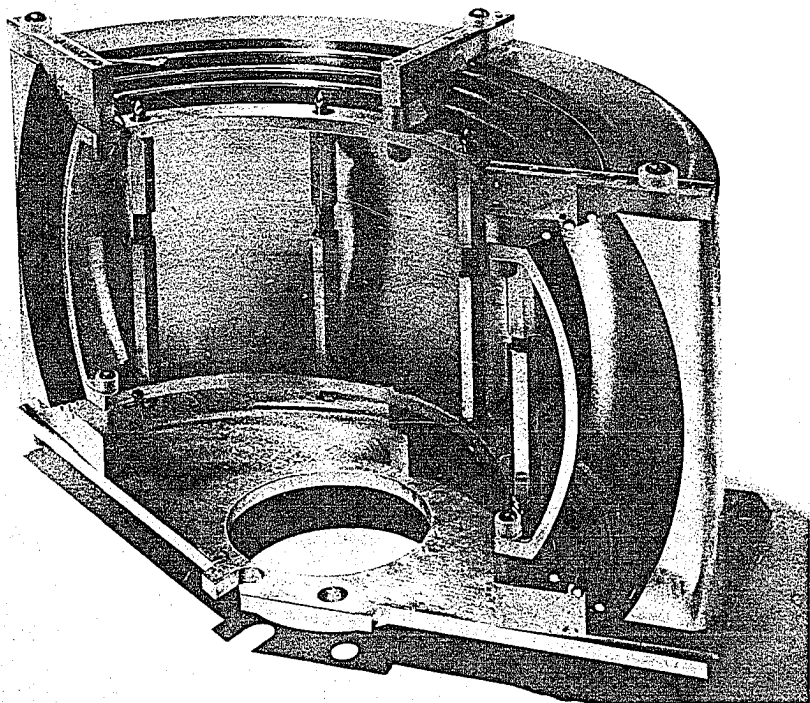


Figure 2. Spherical sector plates.

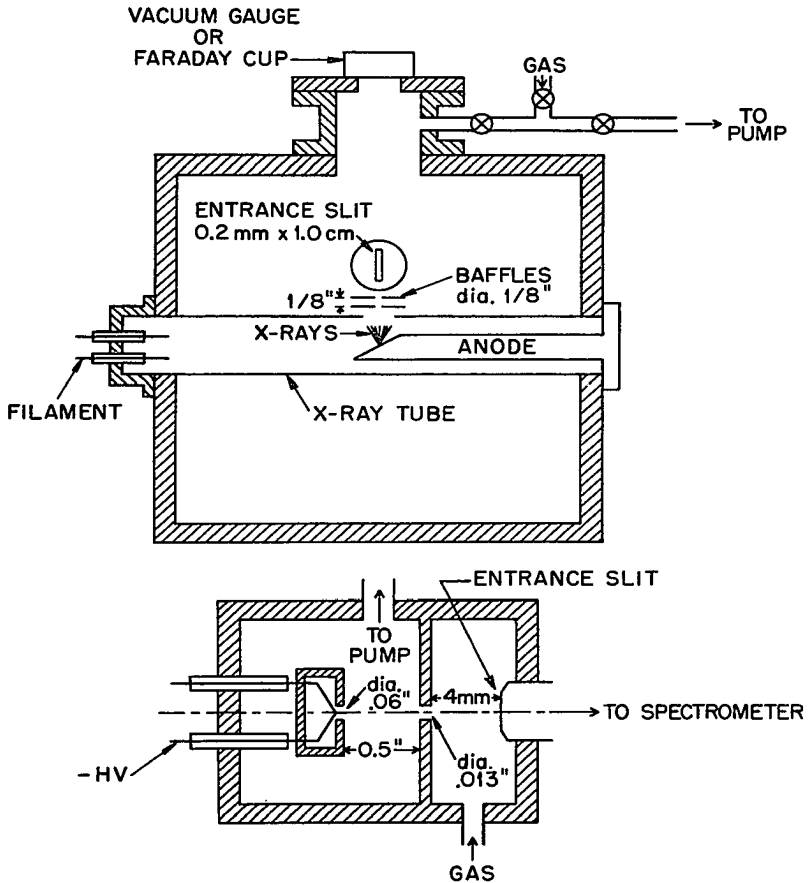


Figure 3. Schematic diagram of target chamber used for gas studies and the electron gun used for inelastic collision studies.

which have the proper kinetic energy determined by the plate voltage pass through the exit slits and strike the electron detector. A scan of the spectrum is accomplished by applying identical sawtooth voltages, but of different polarity, to the spectrometer plates.

X-ray Tube

For all experiments the x-rays used to produce the photoelectrons were generated in the tube shown in Figure 4. The basic parts of the x-ray tube are a tungsten filament, the anode and the window. The tungsten filament, which is at ground potential, is operated with approximately two amperes flowing through it to provide the electrons for the emission current. The operating conditions depend on the anode being used. For the aluminum anode the anode voltage was 8 KV and the emission current was 30 ma, 7 KV and 20 ma was used for the magnesium anode, and 5 KV and 30 ma for the zirconium anode. The anode tip in all cases was cut of an angle of 20° with respect to the spectrometer center line (see Figure 4). Aluminum has a characteristic doublet x-ray $\text{Al } K\alpha_{1,2}$ with an energy of 1486.6 eV and a full width at half maximum (FWHM) of 0.9 eV. Magnesium has a characteristic doublet x-ray $\text{Mg } K\alpha_{1,2}$ at 1253.6 eV with a FWHM of 0.7 eV. There are two other characteristic x-rays associated with Al and Mg that may cause interference. These are the $\text{Al } K\alpha_{3,4}$ and $\text{Mg } K\alpha_{3,4}$ satellites which have an energy 9.5 eV and 7.7 eV respectively larger than the $K\alpha_{1,2}$.⁽²³⁾ The intensities of the $\text{Al } K\alpha_{3,4}$ and $\text{Mg } K\alpha_{3,4}$ satellites are 12% and 9.5% respectively compared to the $K\alpha_{1,2}$. For Zr the characteristic x-ray of interest was the $\text{Zr } M_V\text{-N}_{III}$ (M_C) with an energy of 151.4 eV and a FWHM of 0.77 eV.⁽¹⁴⁾

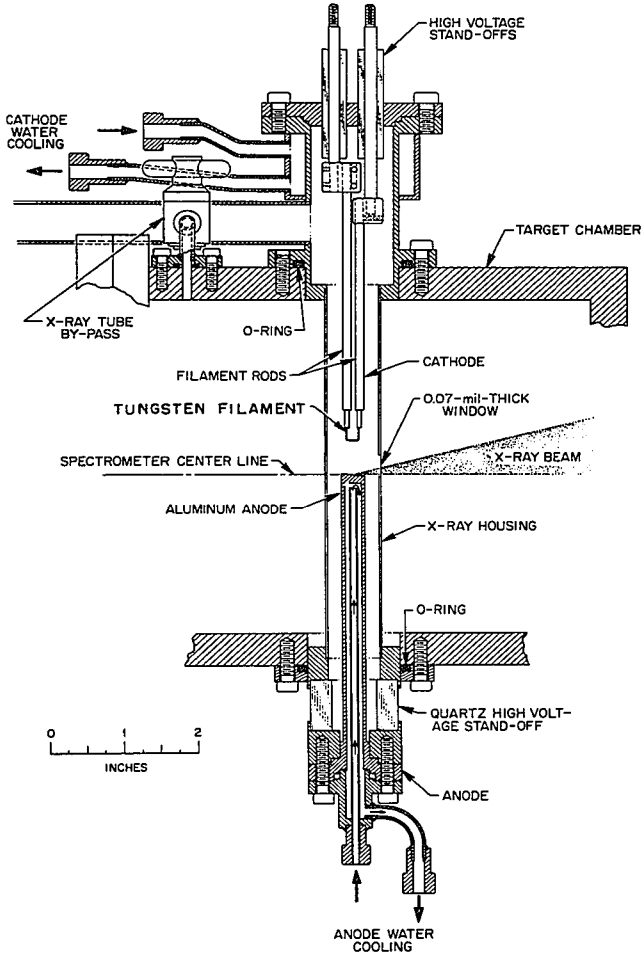


Figure 4. X-ray tube.

The x-rays emitted from the anode pass through a thin window before striking the sample. The window eliminates most of the low-energy bremsstrahlung and stops any stray electrons from the x-ray tube from getting into the spectrometer. These along with electronics, and in the case of solids the secondary electrons, are sources of background noise. In addition, the window allows the differential pumping of the x-ray tube, which must be at lower pressure than the source chamber when used with gases. The vacuum in the x-ray tube is maintained by an oil diffusion pump. The pressure was normally in the low 10^{-7} Torr or high 10^{-8} Torr range.

In the case of the aluminum anode, the window consisted of three layers of aluminum foil giving a total thickness of approximately 0.18 mm. While for the magnesium anode only two layers were used. For the zirconium anode the window was a thin carbon film. The carbon film was made by vacuum depositing graphite ($25-40 \mu\text{gm}/\text{cm}^2$) on a glass slide that had previously been coated with a thin soap film. Normally, the carbon film has small pinholes in it which need to be avoided for the portion of the film used for the window. However, the holes can be seen by placing the slide over a non-glare light and looking with a magnifying glass for the holes. The pinhole free portion is then obtained by floating the film off on top of distilled water. The film is then carefully picked up on a thin, curved metal sheet with a hole cut in it, and dried in a vertical position. It was found that this particular arrangement that a "hard" metal, such as tungsten, worked better than a "soft" metal like indium.

Spectrometer Slits and Plates

The variable entrance and exit slits are 180° apart. Each slit system has a secondary set of slits that define the angle of the beam of electrons being analyzed. For most of the runs the entrance and exit slits were 0.2 mm x 1.0 cm and the entrance and exit baffles were 0.6 mm x 1.0 cm. This gave a resolution of approximately 0.1%.

The plates, shown in Figure 2, are two concentric spherical sectors 5 cm apart. The radii of curvature are 22.5 cm and 17.5 cm, and the sector angles are 145° horizontally and 60° vertically. Fringing fields have been minimized by use of circular rods which can be seen in Figure 2. The spectrometer plates are enclosed in an aluminum housing that contains two slide valves which enable the spectrometer to be sealed off from the target chamber and the detector.

There is a positive potential applied to the inner plate and an identical negative voltage applied to the outer plate. A block diagram of the basic experimental configuration and electronics are shown in Figure 5. The plate voltages are supplied by two Fluke model 412B DC power supplies. The voltage on each plate is calibrated with a Fluke model 817A differential voltmeter. To each plate a sawtooth voltage of the same polarity is superposed on the DC plate voltage. The sawtooth voltages are supplied by a Tektronix 541A oscilloscope and are applied to the plates first through a set of resistors connected in series. By connecting a bypass wire at different points along the series and varying the output position the amplitude of the sawtooth voltage can be changed and thus the energy scan is determined. The sawtooth is synchronized with the channel advance of a 400-channel analyzer by means of a pulse generator which is set for 100 milliseconds.

The x-rays emitted from the anode pass through a thin window before striking the sample. The window eliminates most of the low-energy Bremsstrahlung and stops any stray electrons from the x-ray tube from getting into the spectrometer. These along with electronics, and in the case of solids the secondary electrons, are sources of background noise. In addition, the window allows the differential pumping of the x-ray tube, which must be at lower pressure than the source chamber when used with gases. The vacuum in the x-ray tube is maintained by an oil diffusion pump. The pressure was normally in the low 10^{-7} Torr to high 10^{-8} Torr range.

In the case of the aluminum anode, the window consisted of three layers of aluminum foil giving a total thickness of approximately 0.18

While for the magnesium anode only two layers were used. For the indium anode the window was a thin carbon film. The carbon film was made by vacuum depositing graphite ($25-40 \mu\text{g}/\text{cm}^2$) on a glass slide that had previously been coated with a thin soap film. Normally, the carbon film has small pinholes in it which need to be avoided for the production of the film used for the window. However, the holes can be seen by placing the slide over a non-glare light and looking with a magnifying glass for the holes. The pinhole free portion is then obtained by floating the film off on top of distilled water. The film is then carefully picked up on a thin, curved metal sheet with a hole in it, and dried in a vertical position. It was found that this particular arrangement that a "hard" metal, such as tungsten, worked better than a "soft" metal like indium.

Spectrometer Slits and Plates

The variable entrance and exit slits are 180° apart. Each slit system has a secondary set of slits that define the angle of the beam of electrons being analyzed. For most of the runs the entrance and exit slits were 0.2 mm x 1.0 cm. The entrance and exit baffles were 0.6 mm x 1.0 cm. This gave an estimated resolution of approximately 0.1%.

Figure 2, are two concentric spherical sectors whose radii are 22.5 cm and 17.5 cm, and the sectors are cut 60° horizontally and 60° vertically. Fringing fields are controlled by two circular rods which can be seen in Figure 2. The plates are enclosed in an aluminum housing that contains two slide valves which enable the spectrometer to be sealed off from the target chamber and the detector.

There is a positive potential applied to the inner plate and an identical negative voltage applied to the outer plate. A block diagram of the basic experimental configuration and electronics are shown in Figure 5. The plate voltages are supplied by two Fluke model 412B DC power supplies. The voltage on each plate is calibrated with a Fluke model 817A differential voltmeter. To each plate a sawtooth voltage of the same polarity is superposed on the DC plate voltage. The sawtooth voltages are supplied by a Tektronix 541A oscilloscope and are applied to the plates first through a set of resistors connected in series. By connecting a bypass wire at different points along the series and varying the output position the amplitude of the sawtooth voltage can be changed and thus the energy scan is determined. The sawtooth is synchronized with the channel advance of a 400-channel analyzer by means of a pulse generator which is set for 100 milliseconds.

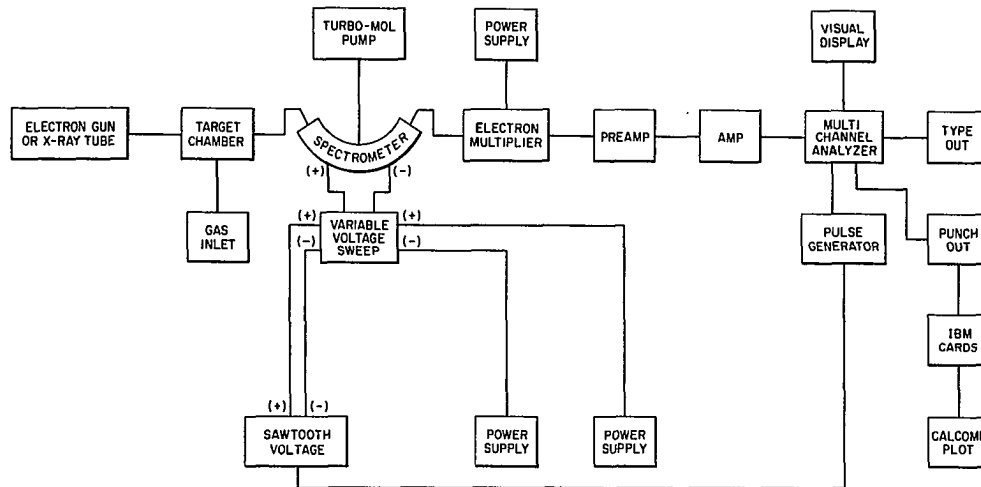


Figure 5. Block diagram of electron spectrometer.

The sweep voltage was typically set to give a 50 eV sweep. The sweep calibration was checked several times preceding, during and following the taking of the data using the following procedure. The plate voltages are set so that a sharp photoelectron or Auger line is located in the last few channels of the analyzer. Then the plate voltages are raised until the same is located in the first few channels of the analyzer. Next, the change in plate voltage is multiplied by the plate constant and divided by the number of channels between the two peak locations.

The plate constant is found by observing two lines of known but of considerably different kinetic energies. Two different runs have to be made with the plate voltages set so that the center of each peak is in the same channel. Then knowing the kinetic energy separation in electron volts and the plate voltage difference, the plate constant can be found. This constant is $(4.057 \pm .002)$ eV/volt.

The electrons of proper kinetic energy passing through the exit slit are post-accelerated by a 50-volt potential before striking the detector. The detector is a Mullard model B419BL channeltron. The signal from the channeltron is amplified and then fed into a multi-channel analyzer where it is stored.

The path of the electrons in the spectrometer, and therefore the energy analysis, is affected by magnetic fields at the spectrometer. Any change in the field during a run will show up either as a broadening of the peak or in some cases as a double peak. Cancellation of the earth's magnetic field and any stray magnetic fields is achieved by using three pairs of mutually perpendicular square Helmholtz coils, each

approximately 2 meters on each side. Two model 313A Fluke power supplies are connected to the coils to supply the proper current. The vertical magnetic field is constantly monitored by a Hewlett-Packard model 3529A magnetometer and the current in the horizontal coils is automatically adjusted by a servo-mechanism to cancel fluctuations in the field.

Experimental Procedure

The gases, liquids and solids were either commercially available or obtained from the ORNL supply. Their purities are given in Table 1. The gas to be studied was allowed to flow into a one liter storage tank, which had previously been pumped down to a pressure of approximately 15μ , until the pressure in the storage tank was approximately one atmosphere. Then by opening a leak valve the gas flowed into the target chamber where the x-rays irradiated the samples. The leak valve was adjusted until the gas pressure in the target chamber was about 10μ while the spectrometer pressure was kept in the 10^{-5} Torr region by continuously pumping with a Sargent-Welch turbomolecular vacuum pump.

The liquids studied in this investigation were poured into a small pyrex test tube and then purified by vacuum distillation. The frozen liquid was then heated up until it vaporized. The vapor was then allowed to flow into the same storage tanks that were used for the gas until the vapor pressure of the liquid was reached. The experimental procedure followed for the liquids (now in the gas phase) was the same as for the gases. The leak valve did have to be heated to keep a uniform flow rate.

Table I
Sample Purity

Ar	>99.9%
Kr	>99.9%
Xe	>99.9%
NO	99.0%
N ₂ O	98.0%
N ₂	99.9%
H ₂ O	Distilled*
CH ₃ I	99.0%
NaCl	99.9%
K Cl	99.9%
K Br	99.7%
Rb Cl	Purified
Cs Cl	99.9%**

*Distilled water from ORNL

**Possibly contaminated by air before loading

The solid samples were prepared as a fine crystal powder which was sprinkled on a tape that had adhesive on both sides. The tape was attached to an aluminum planchet. Four samples were then loaded onto the sample holder, seen in Figure 6, by sliding the planchets into the dove-tailed grooves on the sample holder. The hygroscopic sample CsCl was prepared in a dry box filled with argon to minimize contamination. The transfer chamber, shown in Figure 6, can be sealed by means of a slide valve so that an argon atmosphere can be kept until the chamber is attached to the target chamber.

Sources of Error

There are several sources of error to be considered when analyzing the data. Before taking data, the equipment ought to be checked and calibrations made to make sure everything is working properly. An inconsistent pulse rate from the pulse generator or improperly controlled magnetic field can cause a broadening of a line or in some cases there will be two peaks instead of one. This could be interpreted as a satellite line and must be eliminated as a possibility.

Another possible source of spurious peaks that might be interpreted as satellite lines is contamination of the sample. This possibility can be eliminated by taking several runs and looking for the disappearance or change in intensity of the lines under the same experimental conditions and by looking for other lines characteristic of the possible contaminants. Spurious peaks can be due to either atomic orbitals of other elements or different molecular orbitals of the same element. Chemical shifts often occurring when observing solid samples are too small in the alkali

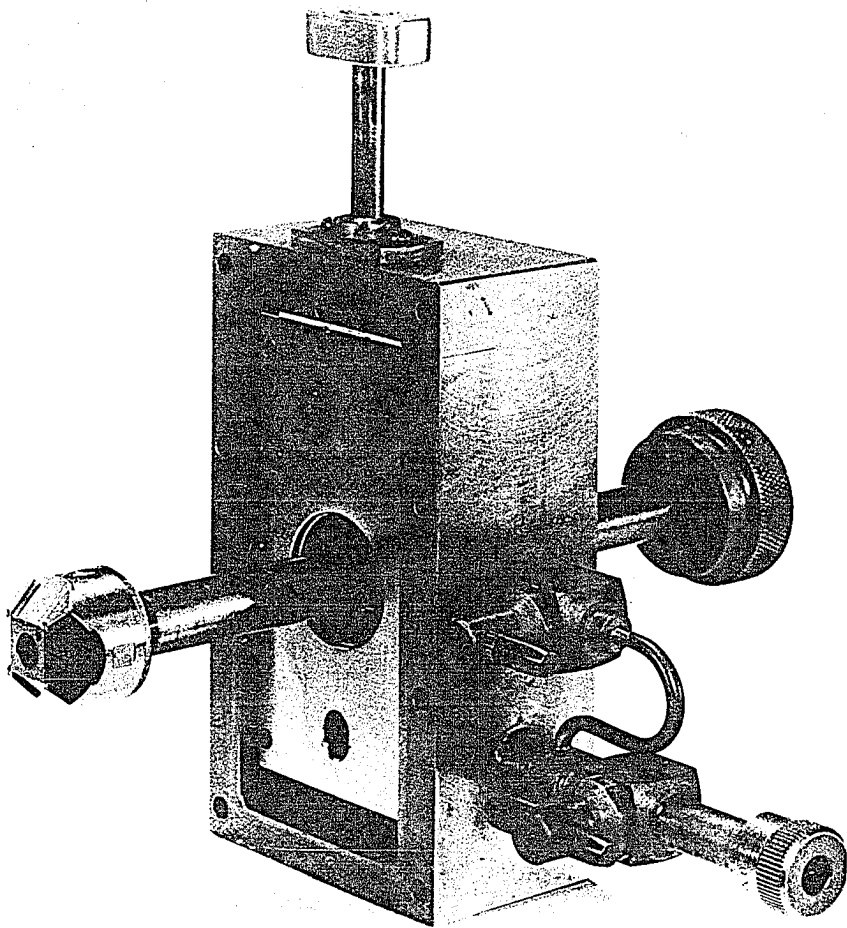


Figure 6. Sample holder and transfer chamber for solids.

metals to be of any bother. To determine if there are any Auger lines present, two different x-ray energies can be used. The kinetic energy of the Auger lines is independent of the excitation source; and by using two different x-ray energies for irradiation, the Auger lines can be identified. Corrections also have to be made for inelastic collision peaks. For gases there are two methods for determining the inelastic collision peaks. Each spectrum can be run several times with the gas at different pressures and observed for the pressure dependence of the peak heights. The other method is to use an electron gun for excitation. The simple electron gun shown in Figure 3 was used for this purpose. The gun was positioned so that the electron path was approximately the same as that of the photoelectrons. The pressure of the gas was the same as for the taking of the photoelectron spectrum.

For the CsCl, the collision loss peak, which is due primarily to a plasmon loss, was subtracted from the satellite region by using the Cl₂s plasmon peak as a reference. An empirical \sqrt{E} dependence⁽²³⁾ on the intensity of the plasmon loss was considered, where E is the kinetic energy of the ejected electron, but was found to make little difference in the corrections.

Most of the background noise for solids is due to secondary electrons. In the case of gases it was found that most of the background noise was due to the electronic equipment.

CHAPTER III

THEORY

A. Sudden Approximation

Earlier studies have shown that the satellite lines seen in the photoelectron spectra of He^(8,9,10,11) and for the most part Ne^(10,12,13,14,15) are explained by invoking the sudden approximation. However, it has been found^(8,10) that when using single electron wave functions the theoretical probability of multiple ionization in the outer shells has been lower than the experimental value. It was pointed out by Byron and Joachain⁽²¹⁾ that for He if electron correlation is considered in the ground state wave function there is excellent agreement between the experimental and theoretical probabilities of multiple ionization. By assuming the excitation to be those of monopole transitions and then using Hartree-Fock wave functions for calculating the satellite separation for inner shell ionization there is good agreement with the experimentally measured energies.

The sudden approximation was initially used for calculation involving excitation following electron impact⁽²⁴⁾ and later used for finding electron shake off probabilities following β decay.^(25,26) Photoionization of a core electron is similar to the situation in β decay and the sudden approximation can be applied.^(27,28,29)

In the sudden approximation it is assumed that there is a sudden change in the Hamiltonian.⁽⁷⁾ This change must happen very fast in

comparison with the period involved in a transition ($\tau \approx \hbar/E_n - E_0$). It is assumed that at $t = 0$, the Hamiltonian suddenly changes from H_1 to H_2 and then remains constant. Before the disturbance, the eigenfunctions are given by

$$\chi = U_i e^{-iE_i^0 t/\hbar} \quad (1)$$

where $H_1 U_i = E_i^0 U_i$. Following the perturbation the eigenfunctions can be denoted by

$$V e^{-iE_f t/\hbar} \quad (2)$$

where $H_2 V_f = E_f V_f$ assuming that at the time of perturbation, $t = 0$ the system is in the i th eigenstate giving

$$\chi = U_i(X) \quad (3)$$

The wave functions must remain continuous at $t = 0$. Expanding the final wave functions as a series of eigenstates, i.e. in a series of solutions of Schrödinger's equation gives at $t = 0$

$$U_i(\bar{X}) = \sum_f C_{fi} V_f(\bar{X}) \quad (4)$$

multiplying by $V_f^*(\bar{X})$ and integrating over all space

$$C_{fi} = \int V_f^*(\bar{X}) U_i(\bar{X}) d\bar{X} \quad (5)$$

and the probability of a transition from state i to f is given by

$$P_{i \rightarrow f} = \left| \int V_f^*(\bar{X}) U_i(\bar{X}) d\bar{X} \right|^2 \quad (6)$$

where the selection rules governing such a transition require that

$$\Delta J = \Delta L = \Delta S = 0 \quad . \quad (7)$$

This shows that following photoionization in an innershell the probability for simultaneously exciting or ejecting an electron from an orbital $n_i l_i j_i$ is given by

$$P_{i, n l j \rightarrow f, n' l' j'} = \left| \int \psi_{f, n' l' j'}^* \psi_{i, n l j} d\psi \right|^2 \quad (8)$$

where $\psi_{i, n l j}$ is the single-electron wave function for the orbital $n l j$ in the ground state of the neutral atom and $\psi_{f, n' l' j'}$ is the single-electron wave function for an ion which does not have to be in the ground state. For a monopole transition l and j have to remain the same but $n \neq n'$. However, it is difficult to describe excited states of an ion and what has usually been done^(8,10,26) is to calculate the probability that an electron will remain in an orbital with the same quantum numbers, i.e. $n = n', l = l', j = j'$ and subtract this from one. Thus

$$P_{i, n l j \rightarrow f, n' l' j} = 1 - \left| \int \psi_{f, n, l, j}^* \psi_{i, n l j} d\psi \right|^2 \quad . \quad (9)$$

If there are N electrons in orbital $n l j$ then Eq. (9) is written

$$P_{i, n l j \rightarrow f, n' l' j} = 1 - \left[\left| \int \psi_{f, n, l, j}^* \psi_{i, n l j} \right|^2 \right]^N \quad (10)$$

or in the final form

$$P_{i, n l j \rightarrow f, n' l' j} = 1 - \left[\left| \int \psi_{f, n l j}^* \psi_{i, n l j} \right|^2 \right]^N - P_f \quad (11)$$

where P_f is a correction⁽²⁷⁾ which arises from the condition that electron shake-up transitions to occupied levels are not physically allowed. The corrections for contributions to filled states can be written

$$P_f = \sum_{n'=1}^X N \frac{N'}{2j+1} \left| \int \psi_{f,n'lj} \psi_{i,nlj} d\tau \right|^2 \quad (12)$$

where $n' \neq n$, and N' is the number of electrons in the orbital designated $n'lj$.

In the case of molecules the sudden approximation should also apply for innershell ionization. The wave function ψ and ψ'_α for a neutral molecule and the ion with a core vacancy on the atom α have been expanded as LCAOs.⁽²⁸⁾ These can be written

$$\psi = \sum_{u=1}^n C_u \phi_u \quad (13)$$

$$\psi'_\alpha = \sum_{u=1}^n K_u \phi'_u \quad (14)$$

where n is the number of orbitals in the basis set in which only valence orbitals are considered. The atomic orbitals ϕ'_u for (α) from which ionization occurs are for the ion whose effective nuclear charge is $Z + 1$, Z being the effective nuclear charge of the neutral atom. The probability for transitions from molecular orbital i of the ground state of the neutral molecular to orbital α of the ion is given from Eq. (8)

$$P_{i \rightarrow f\alpha} = N \left| \sum_{v=1}^n K_{vf} C_{vi} \langle \phi'_v | \phi_u \rangle \right|^2 \quad (15)$$

where N is the number of electrons in the initial ground state orbital $n\ell j$. Using the zero differential overlap (ZDO) approximation, Eq. (15) becomes

$$P_{i \rightarrow f\alpha} = N \left| \sum_{u=1}^n K_{uf} C_{ui} \langle \phi'_u | \phi_u \rangle \right|^2 . \quad (16)$$

Aarons et al⁽²⁸⁾ have calculated the position and intensities of satellite lines, assuming a localized hole approximation, associated with core ionization of several molecules using the above approximations. They were able to get general agreement with experimental results.

B. Configuration-Interaction

When attempting to find a wave function to describe a system it has been pointed out by Slater,⁽³⁴⁾ Kuhn⁽⁶⁾ and Condon and Shortley⁽⁶³⁾ that sometimes several configurations have to be considered simultaneously. If upon photoionization an atom makes a transition from the ground state of the ion to one or more of these allowed excited configurations there will be seen small satellite lines with a higher binding energy than the main photoelectron peak. This mixing of the wave functions can be caused by both electrostatic and magnetic interactions, but the electrostatic is the most important.

The electrostatic interactions are restricted by two selection rules. Only configurations of the same parity ($\sum \ell_i$ is odd or even) and

only states with the same value of J interact. "Even for the strongest configuration interaction, parity and the value of J remain well defined."⁽³⁰⁾ For Russell-Saunders coupling the quantum numbers L and S must remain the same for configuration-interaction transitions. Configuration interaction is a two-electron excitation process. For example, the transition from $4s^2 4p^6 \rightarrow 4s^2 4p^4 4d$ has the selection rules $\Delta L = 1$, $\Delta S = 0$. The process that occurs is (1) a $4s$ electron is ejected into the continuum (2) one of the $4p$ electron refills the $4s$ hole (3) one $4p$ electron goes to the $4d$ subshell.

C. SCF Hartree-Fock

Hartree⁽³⁰⁾ first introduced the method of a "self consistent field" for finding the eigenvalues of a many electron atom. In this it was assumed that the total wave function could be written in the symmetric form as a product

$$\Psi(\bar{r}_1, \bar{r}_2 \dots \bar{r}_z) = \phi_1(\bar{r}_1) \phi_2(\bar{r}_2) \dots \phi_z(\bar{r}_z) \quad (17)$$

Each electron is assumed to move in its own orbital and to be moving in an effective field. Each electron experiences a central potential with an effective charge Z_{eff}

$$Z_{\text{eff}} = Z - \sigma \quad (18)$$

where Z is the nuclear charge and σ is the screening factor for each electron orbital. The principal approximation that is made is the averaging of the potential energy over the angles of \bar{r}_k to make it spherically symmetric. Under these conditions the radial portion can

be separated from the angular and the angular portion can be considered as a constant. This means that only the radial part of the wave function has to be considered when doing the calculations.

Later Fock⁽³¹⁾ used an antisymmetric wave function and the variational technique⁽³²⁾ to arrive at a solution of a many electron system in a manner similar to that of Hartree. The antisymmetric wavefunction is

$$\Psi = \frac{1}{\sqrt{N!}} \begin{vmatrix} \phi_1(1)\alpha(1) & \phi_1(1)\beta(1) & \dots & \phi_n(1)\alpha(1) & \phi_n(1)\beta(1) \\ \phi_2(2)\alpha(2) & \phi_1(1)\beta(2) & \dots & \phi_n(2)\alpha(2) & \phi_n(1)\beta(2) \\ \vdots & \vdots & \ddots & \vdots & \vdots \\ \phi_1(N)\alpha(N) & \phi_1(N)\beta(N) & \dots & \phi_n(N)\alpha(N) & \phi_n(N)\beta(N) \end{vmatrix} \quad (19)$$

where N is the total number of electrons in the system and $N = 2n$. This Slater determinant is made up of n one-electron orbitals. Each orbital is composed of a product of a spatial part and a spin part α and β . Following an outline by Fadley,⁽³³⁾ but only considering the atomic case, and using references (32) and (34), the development of the Hartree-Fock equations are briefly sketched below. The Hamiltonian for an N electron system can be given by

$$H = \underbrace{\frac{-\hbar^2}{2m} \sum_{i=1}^N \nabla_i^2}_{(A)} - \underbrace{\sum_{i=1}^N \frac{Ze^2}{r_i}}_{(B)} + \underbrace{\sum_{i>j}^N \frac{e^2}{r_{ij}}}_{(C)} \quad (20)$$

where the terms are (A) kinetic energy, (B) electron-nucleus interaction (C) electron-electron repulsion. Using the above Hamiltonian and the

variational principle Ψ can be found so that the energy

$$E = (\Psi | H | \Psi) \quad (21)$$

is a minimum, and the Hartree-Fock equations are obtained. The n Hartree-Fock equations then can be used to determine the self consistent orbitals ϕ_i . For electrons at position (1) and position (2) these n equations are

$$\begin{aligned} & \left[-\frac{1}{2} \nabla_1^2 - \frac{Z}{r_{10}} \right] \phi_i(1) \\ & + 2 \left[\sum_{j=1}^n \int \phi_j^*(2) \frac{1}{r_{12}} \phi_j(2) d\tau_2 \right] \phi_i(1) \\ & - \sum_{j=1}^n \left[\int \phi_j^*(2) \frac{1}{r_{12}} (2) d\tau_2 \right] \phi_j(1) = E_i \phi_i(1) \quad . \quad (22) \end{aligned}$$

For simplification the above orbitals now include the spin function

$$\alpha(k), \text{ i.e. } \phi_m(k) \alpha(k) \equiv \phi_m(k) \quad .$$

The last term on the left hand side of Eq. (22) is the exchange interaction term. Exchange interaction is only possible between terms with parallel spin. If the exchange interaction term is multiplied and divided by $\phi_i^*(1) \phi_i(1)$ Eq. (22) can, in atomic units, be given by

$$\begin{aligned}
 & \left[-\frac{1}{2} \nabla_1^2 - \frac{Z}{r_1} \right] \phi_i(1) \\
 & + 2 \left[\sum_{j=1}^n \int \phi_j^*(2) \frac{1}{r_{12}} \phi_j(2) d\tau_2 \right] \phi_i(1) \\
 & - \left[\frac{\sum_{j=1}^n \int \phi_i^*(1) \phi_j^*(2) \frac{1}{r_{12}} \phi_i(2) \phi_j(1) d\tau_2}{\phi_i^*(1) \phi_i(1)} \right] \phi_i(1) \\
 & = \epsilon_i \phi_i(1) \quad . \quad (23)
 \end{aligned}$$

This revised form of the Hartree-Fock equation shows that $\phi_i(1)$ is a solution of a Schrödinger equation with a Hamiltonian operator which is a sum of several parts. These are (1) the kinetic energy, (2) the potential energy in the field of the nucleus, (3) the potential energy in the field of N electrons minus a correction term due to exchange interaction. The exchange interaction term corrects for the interaction of the particle with itself⁽³⁴⁾ which is erroneously included in the third term of Eq. (23). The correction term may be regarded as representing the potential energy, at the position 1 of the electron in question, of a charge distribution at point 2, of magnitude

$$\sum_j \frac{\phi_i(1) \phi_j(2) \phi_j(1) \phi_i(2)}{\phi_i^*(1) \phi_i(1)} \quad . \quad (24)$$

Equation (23) is in the general form of an eigenvalue equation

$$F \phi_i = E_i \phi_i$$

where F is the Hartree-Fock Hamiltonian operator. By defining the kinetic, coulomb and exchange operators G_i , J_j and K_j

$$G(1) = - \frac{1}{2} \nabla_1^2 + \frac{Z}{r_1} \phi_i(1) \quad (26)$$

$$J_j \phi_i(1) = \int \phi_j^*(2) \frac{1}{r_{12}} \phi_i(1) \phi_j(2) d\tau_2 \quad (27)$$

$$K_j \phi_i(1) = \int \phi_j^*(2) \frac{1}{r_{12}} \phi_i(2) \phi_j(1) d\tau_2 \quad (28)$$

writing for the expectation values G_i , J_{ij} and K_{ij}

$$G_i = \langle \phi_i(1) | G(1) | \phi_i(1) \rangle = \int \phi_i(1)^* \left(-\frac{1}{2} \nabla_1^2 - \frac{Z}{r_1} \right) \phi_i(1) d\tau \quad (29)$$

where G_i is in the form of a screened hydrogenic potential,

$$\begin{aligned} J_{ij} &\equiv \langle \phi_i(1) | J_j | \phi_i(1) \rangle \\ &= \iint \phi_i^*(1) \phi_j^*(2) \left| \frac{1}{r_{12}} \right| \phi_j(2) d\tau_1 d\tau_2 \end{aligned} \quad (30)$$

$$\begin{aligned} K_{ij} &\equiv \langle \phi_i(1) | K_j | \phi_i(1) \rangle \\ &= \iint \phi_i^*(1) \phi_j^*(2) \frac{1}{r_{12}} \phi_i(2) \phi_j(1) d\tau_1 d\tau_2 \end{aligned} \quad (31)$$

Now using Eqs. (29), (30), and (31) E_i is given by

$$E_i = \langle \phi_i(1) | F | \phi_i(1) \rangle = G_i + \sum_{j=1}^n (2 J_{ij} - K_{ij}) \quad (32)$$

To solve for E_i the usual approach is to use an iterative procedure. First, an orbital ϕ_i is chosen that is an eigenfunction of Eq. (32). What is normally done is to assume that ϕ_i is an eigenfunction of a screened hydrogenic potential. Then calculate E_i' to get an initial estimate of the energy. Adjust ϕ_i by varying parameters and calculate a new E_i^v . Keep adjusting ϕ_i and comparing energies E_i^m with E_i^{m+1} until a minimum is found. Do this for all orbitals and sum the E_i to give the total energy E

$$E = 2 \sum_{i=1}^n G_i + \sum_{i,j}^n (2 J_{ij} - K_{ij}) \quad (33)$$

The calculations for inner shell ionization of the rare gases were made by C. W. Nestor, Jr.* using a Hartree-Fock Program written by C. Froese-Fischer. (35)

To calculate the approximate change in the binding energy due to a shake-up transition, first calculate the total energy of the ion in the ground state using Eq. (33), second, calculate the total energy of the ion in the excited state and subtract the two energies. In doing this it is assumed that the orbitals ϕ_i for the ground state of the ion are identical to the orbitals $\phi_i(\text{excited})$ of the excited ion.

*Dr. C. W. Nestor, Jr. of the Mathematics Division of Oak Ridge National Laboratory.

CHAPTER IV

RARE GASES AND ALKALI METAL IONS

Inner Shells of the Rare Gases

The first topic to be discussed in this chapter is the satellite structure seen in photoelectron spectra of the inner shells. The spectra resulting from inner shell photoionization of Ar, Kr, and Xe are shown in Figures 7, 8, and 9 respectively. The photoelectron spectrum of the Cs4d is shown in Figure 10 to compare the satellite structure to that of the Xe4d spectrum. Also, the photoelectron spectra of the I3d and I4d of methyl iodide shown in Figure 11 is compared with the Xe3d and Xe4d shown in Figure 9. These can be compared with the Xe3d and Xe4d since Cs^+ and I^- are isoelectronic with Xe. In the case of the photoelectron spectra of the inner shells the energy separation and relative intensities of the satellite lines are expected to be almost independent⁽²⁷⁾ of the individual shell being considered. The analysis of the inner shell satellite lines is given in Table II. In Figure 7 it can be seen that there is some difference in the spectra of Ar2p and Ar2s. In the case of Ar2p there are two main contributions to the satellite area, with the average separation from the Ar2p_{3/2} being 25.1 eV. The satellite structure associated with Ar2s is located 23.6 eV from the Ar2s. Also, the relative intensity of the satellite lines for the Ar2p is slightly less

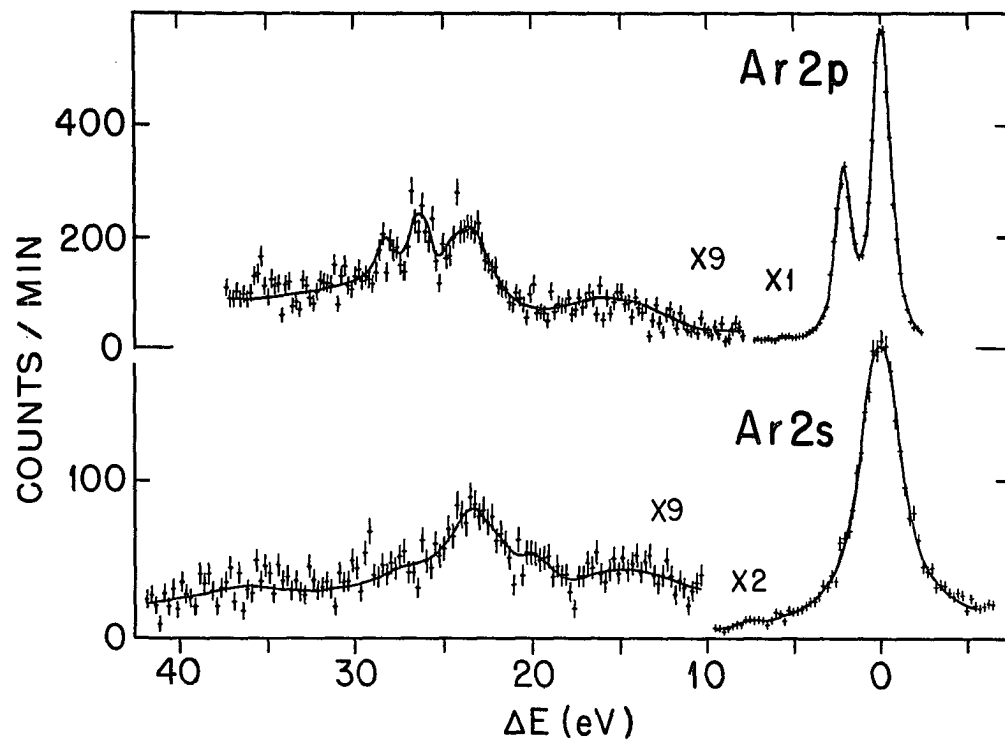


Figure 7. Photoelectron spectra of Ar2s, Ar2p and associated satellite structures using $MgK\alpha$ x-rays.

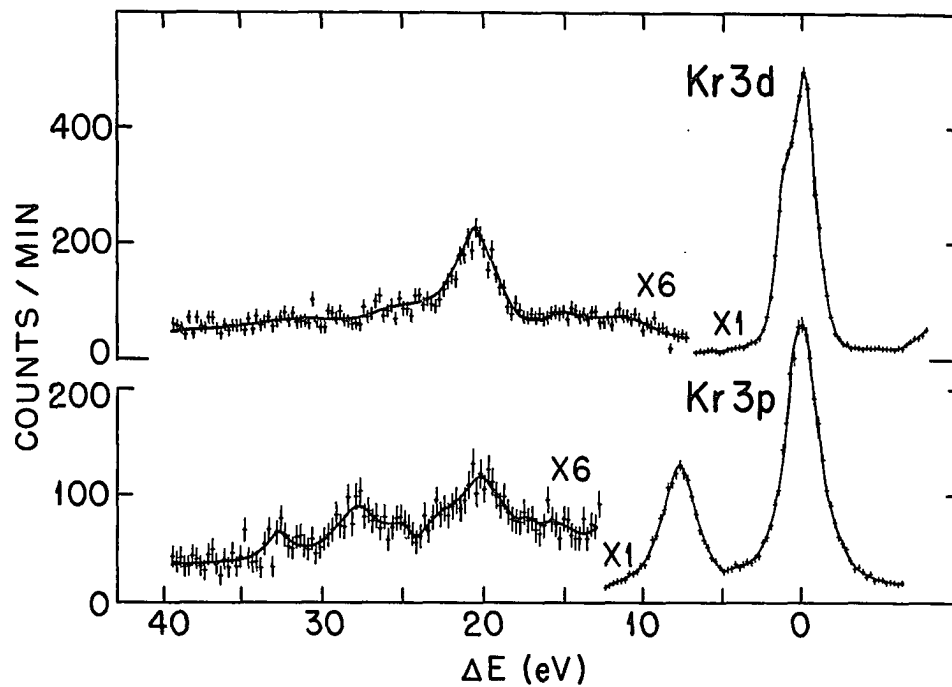


Figure 8. Photoelectron spectra of Kr3p, Kr3d and associated satellite structures using MgK_{α} x-rays.

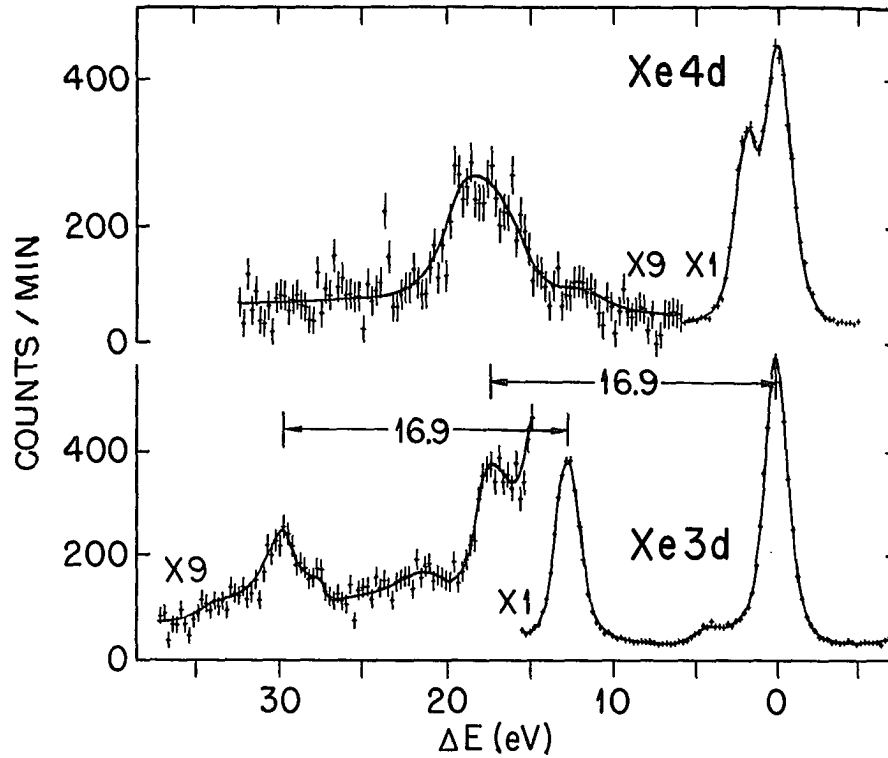


Figure 9. Photoelectron spectra of Xe3d, Xe4d and associated satellite structures using $M_gK\alpha$ x-rays respectively for irradiation.

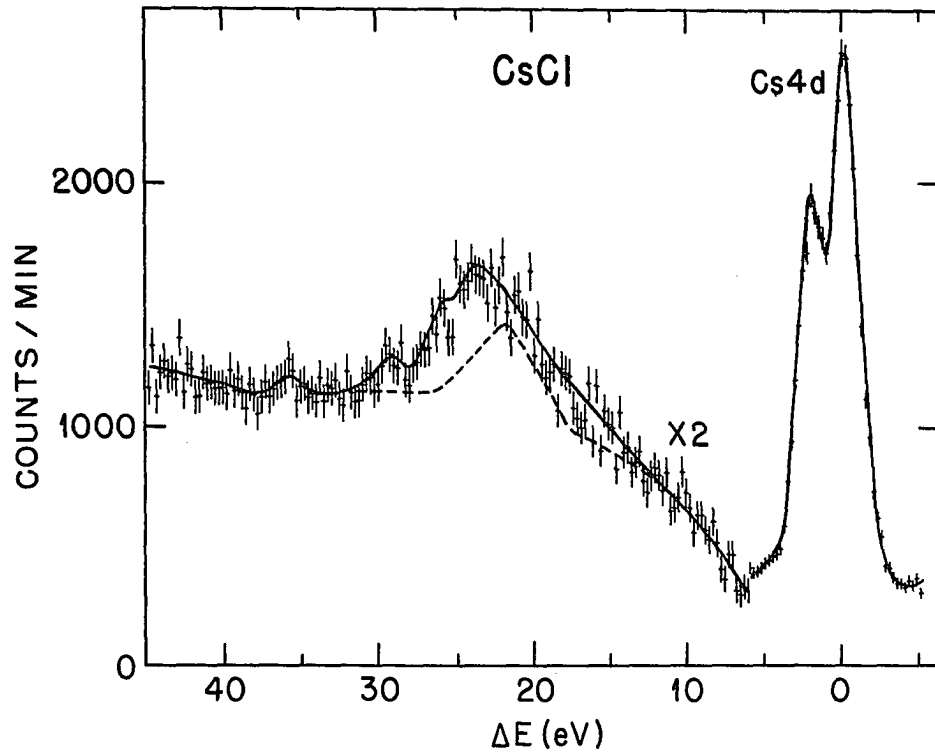


Figure 10. Photoelectron spectra of Cs4d in CsCl and associated satellite structure using $M_g K\alpha$ x-rays.

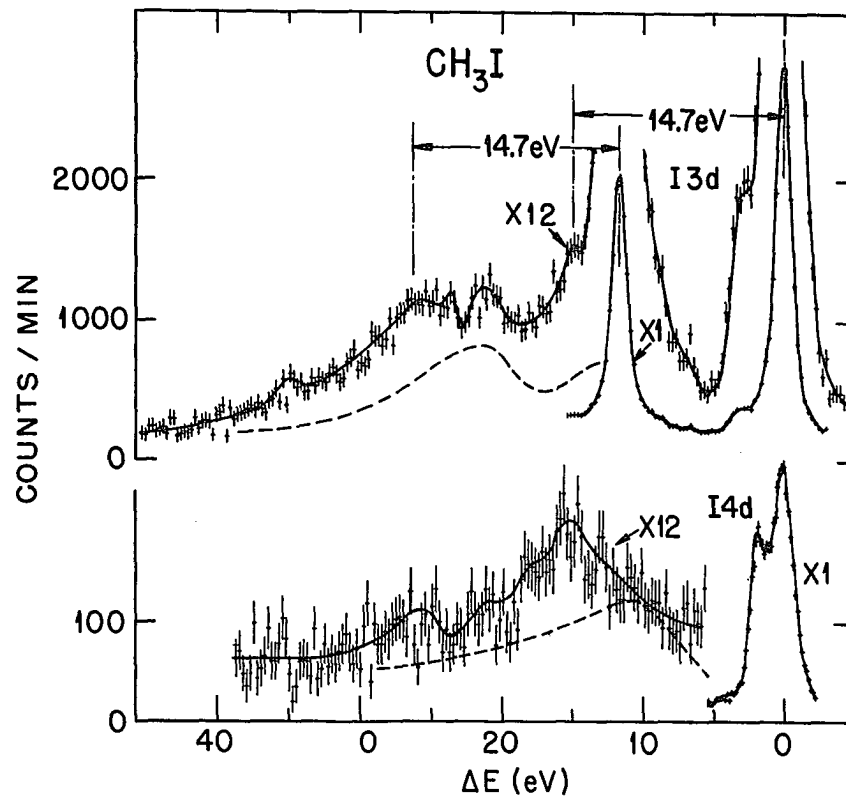


Figure 11. Photoelectron spectra of $\text{I}3d$, $\text{I}4d$ and CH_3I and their associated satellite structures using $\text{M}_g\text{K}\alpha$ x-rays.

Table II

Excitation Energy and Intensities of Satellite Structure in the Photoionization of Core Shells of the Rare Gases

Inner shell Vacancy	E_B (a)	E_e (b)	Intensity		Excitation Energy (eV)	
			Exp ^(d)	Theory ^(e)	Exp ^(f)	Theory ^(g)
Ne 1s	870.2	617	8.7±0.7	19.6	38.8±0.3 ^(h)	37.6
Ne 1s		384	9.6±0.7	19.6	39.0±0.3 ^(h)	37.6
Ar 2s	326.3			14.6		
		927	8.4±1	14.6	23.6±0.3	22.2
		604	10 ±2 ^(c)	14.6		
Ar 2p	248.5	1238	6.7±1	15.4	25.3±0.3	20.9
		1005	7.3±1	15.4	24.9±0.3	20.9
		681	7 ±2 ^(c)	15.4		
Kr 3p	214.4	1272	5.8±1	11.6	20.5±0.3	-
		1039	5.4±1	11.6	20.2±0.3	-
Kr 3d	93.7	1393	8.0±1	11.5	20.4±0.3	18.8
Kr 3d		1160	8.3±1	11.5	20.4±0.3	18.8
Xe 3d _{3/2}	689.0	798	11 ±1	12.4	16.9±0.3	15.9
		565	8 ±1	12.4	16.9±0.3	15.9
Xe 3d _{5/2}	676.4	810	10.7±1	12.4	16.9±0.3	15.9
		577	8.4±1	12.4	16.9±0.3	15.9
Xe 4d _{5/2}	67.5	1419	6.3±0.5	9.6	17.0±0.3	-
		1186	5.1±0.5	9.6	16.9±0.3	-
		84	5.7±1	9.6	16.8±0.3	-
CH ₃ I						
I 3d _{5/2}	~620	~634	~15		14.7±0.3	-
I 4d	~50	~1204	~12		15.1±0.5	-
CsCl						
Cs 4d _{5/2}	~77	~1177	~13		23.3±0.5	-

(a) Binding energies taken from Siegbahn et al. (13). In the case of Ar2p, Kr3p, Kr3d and Xe4d the binding energy for the $\ell+1/2$ subshell is given.

Table II (continued)

-
- (b) Photoelectron energies. The following x-ray energies were used: 1487 eV, 1254 eV, 930 eV, and 151 eV.
- (c) Data taken with $\text{CuL}\alpha$ x-rays as obtained by O. Keski-Rahkonen and M. O. Krause (unpublished data).
- (d) Total intensity of satellite structure relative to normal photoelectron peak = 100.
- (e) Calculation of total electron shake-up + shake-off for the outermost p shell (cf. Carlson and Nestor, ref. 27) relative to normal photoelectron peak = 100.
- (f) As measured for peak of normal photoelectron peak to peak of satellite structure.
- (g) Calculations of difference of total energies between the free atom and the excited state of ion using non-relativistic Hartree-Fock program of C. F. Fischer. Calculations made by C. W. Nestor, Jr. The ions had the indicated vacancy in the core shell and the outer shell np electrons were excited to the $(n + 1)$ p shell.
- (h) Average of energy peaks corresponding to $2p^5 3p$ (up), $2p^5 3p$ (down). (Cf. refs. 10,13).

than the intensity of the shake-up peaks associated with Ar2s. This is in agreement with the results of Krause and Keski-Rahkonen⁽³⁶⁾ using $\text{CuL}\alpha_{1,2}$ x-rays for excitation, where the relative intensity difference is slightly more than for the $\text{MgK}\alpha$ x-rays (cf. Table II).

In the case of the inner shell spectra of Kr shown in Figure 8 the spectra of the Kr3d and Kr3p are very similar. The separation of the main satellite lines from Kr3d and Kr3p are approximately the same. Both satellite structures associated with these two photoelectron peaks have a main peak with a small contribution with a slightly higher binding energy. The main satellite peaks of both the Kr3p and Kr3d are located approximately the same distance from the normal photoelectron peak.

The spectra of the Xe3d and Xe4d photoelectron lines, seen in Figure 4, again show the similarity of the inner shell shake-up peaks. The satellite peaks have the same separation from the main photoelectron line for both the 3d and 4d. The relative satellite intensity for the Xe3d is significantly higher than that associated with the Xe4d, and fall outside the error limits given in Table II. As with the shake-up peaks in the spectra of the inner shells of Ar and Kr there is seen to be multiple structure in the satellite lines of Xe3d. None was observed in the Xe4d and may be because of the low intensity and resultant poor statistics. From the sudden approximation it follows that the probability of electron shake-up should be independent of the photon energy as long as it is high enough to be in the region covered by the approximation. Also, since the removal of a core electron changes the central potential by approximately the same amount regardless of which core is involved,

the probability for electron shake-up will be independent of the core vacancy.

We can use Table II to compare the above generalizations with the data. First considering the independence of shake-up probability on photon energy there is seen to be no general trend in the case of the $MgK\alpha$ and $AlK\alpha$ x-rays. Also, even for the $ZrM\zeta$ x-ray 151.4 eV there is seen to be no energy dependence in the case of $Xe4d$. There is not seen to be any strong dependence for the $CuL\alpha_{1,2}$ x-rays.⁽³⁶⁾ Earlier studies⁽⁶²⁾ were made of electron shake-off from the L shell as a result of photoionization in the K shell of neon as a function of photoelectron energy. The probability for shake off remained constant from photoelectron energies of 100 eV up to 17.5 keV. Below 100 eV the shake-off probability rapidly decreased. At 65 eV above the Nels binding energy the shake-off intensity dropped to 20% of its maximum, but the shake-up probabilities were nearly unchanged from those taken at higher photon energies. Thus the shake-up probability associated with inner shell ionization is fairly consistent, for Ne through Xe, as expected from the sudden approximation.

As mentioned previously in Chapter III it is difficult to calculate the probability of shake-up because of the problems of trying to determine the wave functions of ions in excited states. Specific calculations⁽¹²⁾ are available, however, for the excitation of neon into the $1s2s^22p^53p^2S$ level. Because the calculations of shake-up alone are difficult the total probability shake-up + shake-off is calculated using Eq. 11 in Chapter III. The calculated probabilities⁽²⁷⁾ of shake-up + shake-off are given in Table II. It is interesting to note that the calculations suggest a slightly higher probability of shake-up

following photoionization in the Xe3d shell than in the Xe4d, and as noted earlier this is consistent with the observed results. This is due to the fact that as an electron is removed from shells of lower principal quantum number the effective change in the charge of the nucleus, Z , increases and ΔZ approaches one.

Second, let us consider the energy of excitation due to electron shake-up. The measured energies of excitation and those calculated by taking the energy difference between the ground state and the most likely monopole excited configuration of the ion are listed in Table II.

The first monopole excited level would involve the excitation of an outer p electron. The excitation energies listed are the average of the configuration. The calculations were carried out by C. W. Nestor, Jr.⁽²⁷⁾ using a program written by Fischer.⁽³⁵⁾ In Table II the theoretical and experimental monopole excitation energies are observed to be, for the most part, in good agreement. The trends in the separation are in excellent agreement. The theoretical energies however, are consistently lower than those observed and this is probably due to the fact that electron correlation is neglected in the theoretical calculations.

The alkali metal cesium when singly ionized is isoelectronic with xenon and one would expect the photoelectron spectra of identical shells to be similar. CsCl was used in order to compare the spectrum of the Cs4d to that of the Xe4d (cf. Figures 9 and 10). The similarity in the spectra can be easily seen by comparing the Cs4d and Xe4d. The relative satellite intensity is more for the Cs4d than for either the Xe3d or

Xe4d. The large error listed in Table II for the shake-up intensity in the case of Cs4d is due to the difficulty in determining the extent of the plasmon peak. Also, the separation of the Cs4d shake-up peak from the normal photoelectron line is more than that of the Xe4d or Xe3d.

The photoelectron spectra of inner shells of iodine, which has an atomic number ($Z = 53$) one less than that of Xe, were also taken. The molecule CH_3I was used because it has a high enough vapor pressure to be studied in the gas phase.

Both the I3d and I4d photoelectron spectra are shown in Figure 11. As can be seen the I3d and I4d main satellite lines are located at approximately the same positions. There are also indications of other relatively large lines in addition to the main shake-up peaks. The energies are such that they cannot be due to Auger lines in the case of both the I3d and I4d. The satellite lines in the I3d spectrum start at 14.7 eV and show a continuous contribution out to at least 23.5 eV. Observing the I4d it looks as if the $\text{I}3d_{5/2}$ and $\text{I}3d_{3/2}$ may have overlapping satellite lines. This would explain not seeing a sharp peak located 14.7 eV from the $\text{I}3d_{3/2}$. The width of the peak at 21.0 eV in the I3d photoelectron spectrum indicates that it is made up of two unresolved lines. The spectrum of the I4d is similar to the I3d with regard to both the distribution of the satellite lines and their relative intensities. The relative shake-up intensity of the satellite lines for the I3d and I4d are 15.2% and 12.5% respectively.

Comparing the inner shell photoelectron spectra of iodine, xenon, and Cs^+ (cf. Figures 9, 10, and 11 and Table II) there is seen to be a trend to higher satellite separation from the normal photoelectron peak

as the atomic number increases. There is no trend observed in the satellite lines relative intensities as a function of the atomic number. Both the iodine and cesium ions photoelectron spectra have higher relative intensities than that of xenon which is probably because of the different chemical environment.

Satellite Lines in the X-Ray Photoelectron Spectra of the Outer Shells

There have been several studies of the outer shells of the rare gases. The satellite lines of He^(9,10) and those found in the spectra of the outer shells of Ne^(10,13) have been attributed to monopole excitations. Recently Wuilleumier and Krause⁽¹⁴⁾ have made a very thorough angular and energy-dependent study of Ne and concluded that most of the satellite lines are due to monopole excited states and that the contribution due to configuration-interaction is "small if not negligible."

The outer shells of Ar were also previously studied.⁽¹⁰⁾ The satellite peaks were attributed to monopole excited states but with discrepancies shown between the experimentally measured energies and those calculated using the optical data.⁽¹⁸⁾

Our measurement of the spectra of the outer shells of Ar, Kr, and Xe are shown in Figures 12 through 17. An analysis of the data is given in Table III. An analysis of the satellite lines in the spectra of the alkali metal ions is given in Table IV. The spectra of the outer shells of several alkali metal ions were rerun⁽¹⁶⁾ in order to compare the data to those of the isoelectronic rare gases. A comparison of the Kr4p,4s photoelectron spectra of Rb⁺ and Kr are given in Figure

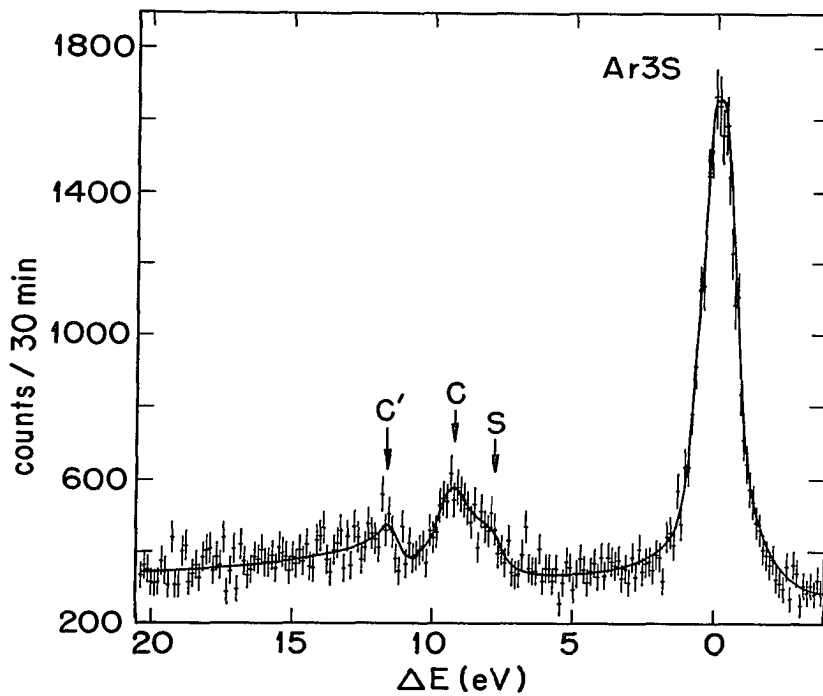


Figure 12. Photoelectron spectrum of Ar3s and associated satellite structure using $MgK\alpha$ x-rays.

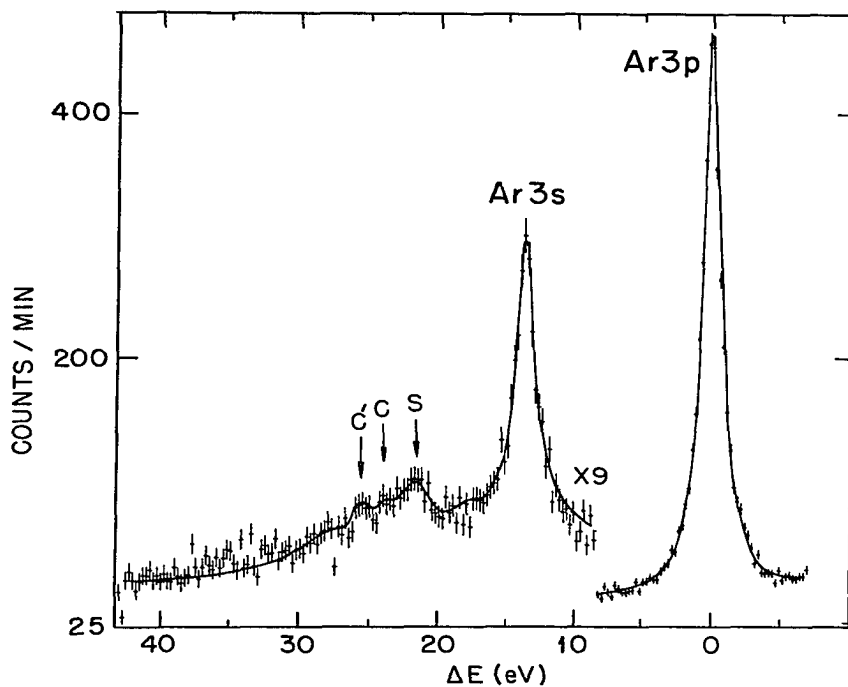


Figure 13. Photoelectron spectra of Ar3p, Ar3s and their associated satellite lines using the $ZrM\zeta$ x-ray.

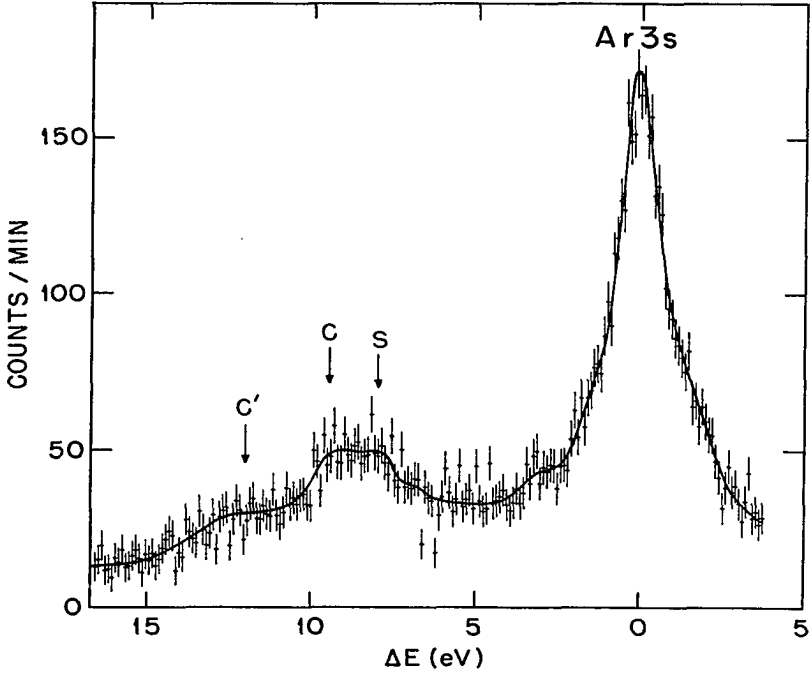


Figure 14. Photoelectron spectrum of Ar3s showing associated satellite lines of the Ar3s and Ar3p using the $ZrM\zeta$ x-ray.

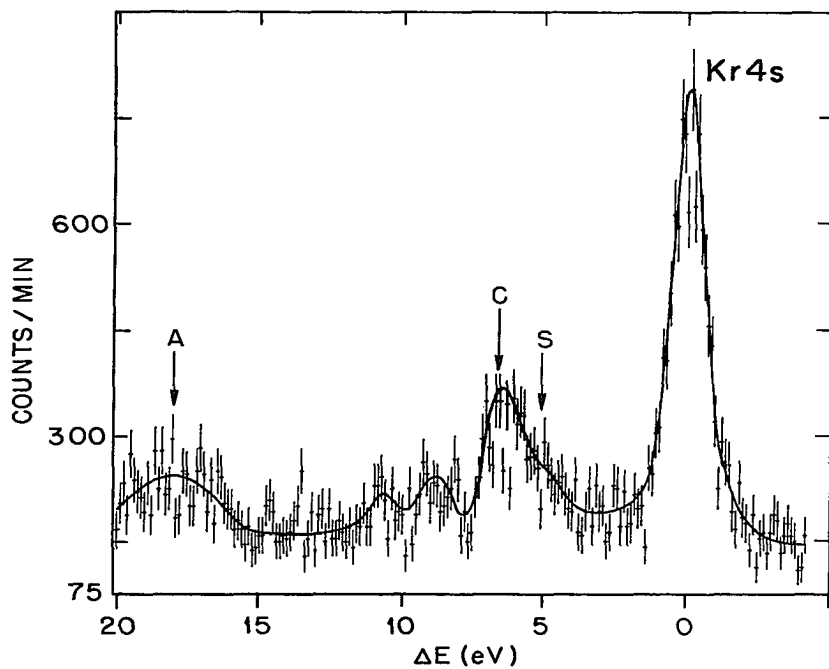


Figure 15. Photoelectron spectrum of Kr4s and associated satellite lines using $M_gK\alpha$ x-rays.

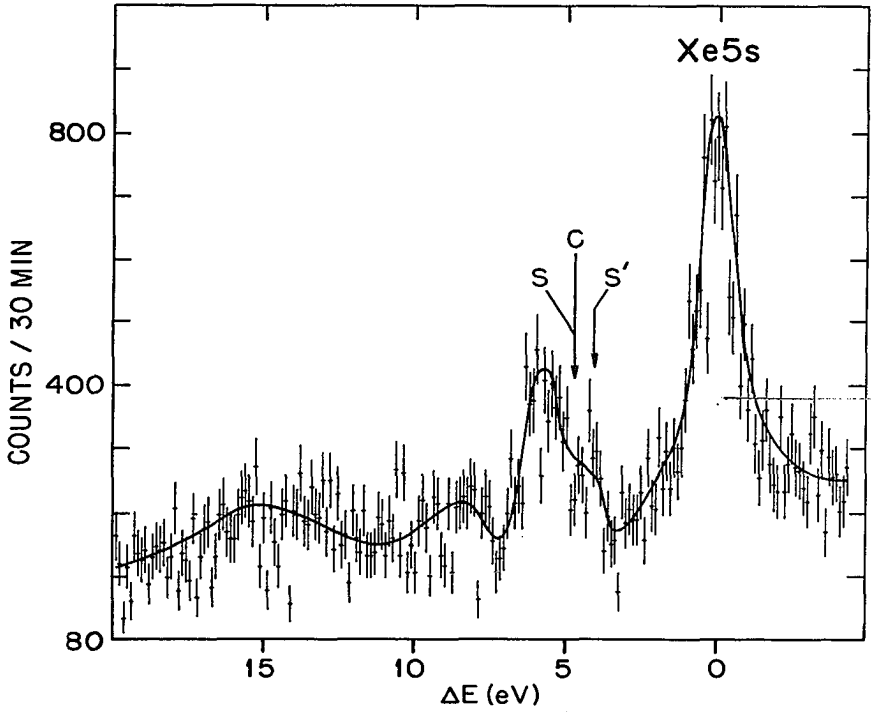


Figure 16. Photoelectron spectra of Xe5s and associated satellite lines using $MgK\alpha$ x-rays.

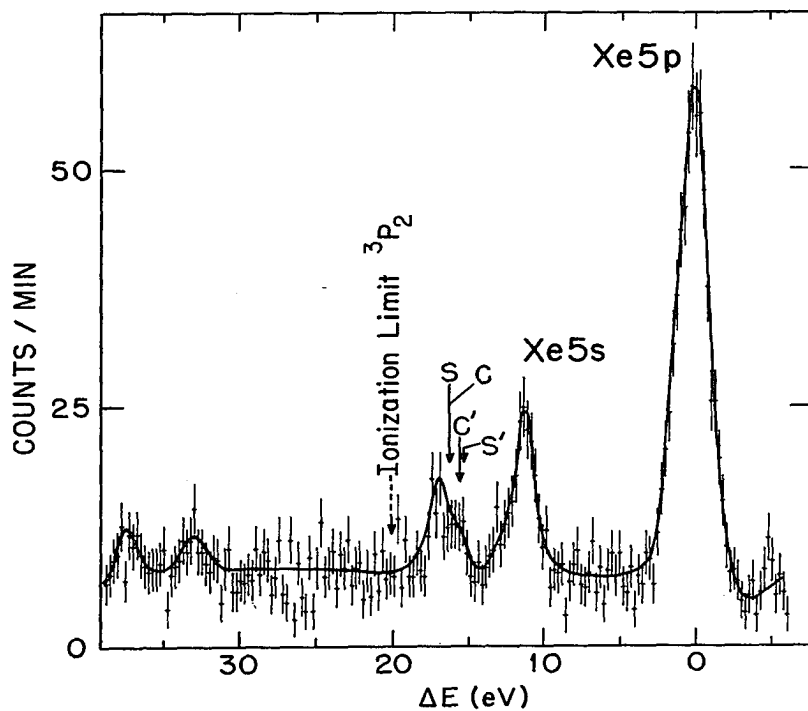


Figure 17. Photoelectron spectra of Xe5p, Xe5s and their associated satellite lines using $M_gK\alpha$ x-rays.

Table III

Excitation Energy and Intensities of Satellite Structure in the Photoionization of Outer Shells of the Rare Gases

Line	Excitation Energy		Configuration	Intensities ^(c)		
	XPS ^(a)	Optical ^(b)		AlK $\alpha_{1,2}$	MgK $\alpha_{1,2}$	ZrM ζ
Ar 3p	0	0	3s ² 3p ⁵ ² P ^o	145±8	182±10	553±25
Ar 3s	13.5±0.1	13.49	3s3p ⁵ ² S	100	100	100
S	21.6±0.2	21.39	3s ² 3p ⁴ 4p 4p' ² P ^o	3±2	4±2	15±3
C	22.9±0.1	22.82	3s ² 3p ⁴ 3d 3d' ² S	19±2	15±2	15±2
C'	25.4±0.2	25.44	3s ² 3p ⁴ 4d 4d' ² S	6±3	7±3	8±3
Kr 4p	0	0	4s ² 4p ⁵ ² P ^o		466±25	
Kr 4s	13.5±0.1	13.51	4s4p ⁵ ² S	100	100	
S	18.4±0.2	18.61	4s ² 4p ⁴ 5p 5p' ² P ^o	7±3	9±3	
C	20.0±0.1	19.94	4s ² 4p ⁴ 4d 4d' ² S	31±6	25±3	
C'		20.39	4s ² 4p ⁴ 6s 6s' ² S	--	--	
Xe 5p	0	0	5s ² 5p ⁵ ² P ^o	355±20	449±20	
Xe 5s	11.3±0.1	11.27	5s5p ⁵ ² S	100	100	
S'		15.37	5s ² 5p ⁴ 6p 6p' ² P ^o	11±3	10±3	
C		16.02	5s ² 5p ⁴ 5d 5d' ² S	--	--	
S		16.27	5s ² 5p ⁴ 6p 6p' ² P ^o	--	--	
--	16.9±.2	--	---	62±7	45±5	

(a) XPS data taken from Figures 12 through 16 and averaged with data of similar runs. Energy is given relative to normal photoelectron peak corresponding to photoionization in the outermost p shell.

(b) Energy difference as obtained from optical data (C. E. Moore, Atomic Energy Levels, Vols. I, II and III, NBS 467, U. S. Govt. Printing Office, Washington, D. C., 1949, 1952 and 1958). Energies are given for the corresponding configuration.

(c) Intensities of peaks obtained in XPS data using AlK α , MgK α and ZrM ζ x rays at 1486.6 eV, 1253.6 eV and 151.4 eV respectively. Intensities are given relative to normal photoelectron peak corresponding to photoionization in the outermost s shell.

(d) Energy difference as obtained from optical data (Cf. ref. 42).

Table IV

Analysis of Satellite Structure in the Photoelectron Spectra
of the s and p Shells of the Alkali Metal Ions

Compound	Line	Excitation Energy		Configuration	Intensities (c)	
		XPS (a)	Optical (b)		AlK $\alpha_{1,2}$	MgK $\alpha_{1,2}$
NaCl	Na ⁺ 2s		32.8	2s ² 2p ⁶ ² S	100	
	Na ⁺ 2p		0	2s ² 2p ⁵ ² P ^o	41±4	
KBr	K ⁺ 3p	0	0	3s ² 3p ⁵ ² P ^o	231±23	
	K3s	16.0±0.2	16.19	3s3p ⁵ ² S	100	
	C	29.8±0.3	29.96	3s ² 3p ⁴ 4s 4s'' ² S	71±18	
	C		31.1	3s ² 3p ⁴ 3d 3d' ² S		
	S		not listed	3s ² 3p ⁴ 4p 4p' ² P ^o		
KCl	K ⁺ 3p	0	0	3s ² 3p ⁵ ² P ^o	229±23	
	K ⁺ 3s	16.1±0.2	16.19	3s3p ⁵ ² S	100	
	C		29.96	3s ² 3p ⁴ 4s 4s'' ² S	39±8	
	C		31.1	3s ² 3p ⁴ 3d 3d' ² S		
	S		not listed	3s ² 3p ⁴ 4p 4p' ² P ^o		
RbCl	Rb ⁺ 4p	0	0	4s ² 4p ⁵ ² P ^o	399±40	412±40
	Rb ⁺ 4s	15.9±0.2	16.2	4s4p ⁵ ² S	100	100
	C	26.0±0.3	26.61	4s ² 4p ⁴ 4d 4d' ² S	63±10	64±10
	C		25.30	4s ² 4p ⁴ 5s 5s'' ² S		
	C		32.8 ^(d)	4s ² 4p ⁴ 5d ² S		
	S		not listed			
CsCl	Cs ⁺ 5p	0	0	5s ² 5p ⁵ ² P ^o	275±25	
	Cs ⁺ 5s	12.9±0.3	15.84	5s5p ⁵ ² S	100	
	C	22.2±0.4			117±20	

(a) Data taken from x-ray photoelectron spectra of the corresponding salts. Energy is given relative to normal photoelectron peak corresponding to photoionization in outermost p shell of alkali metal ion.

(b) Energy difference as obtained from optical data for singly charged alkali metal ion. (C. E. Moore, Atomic Energy Levels, Vols. I, II and III, NBS 467, U. S. Govt. Printing Office, Washington, D. C., 1949, 1952 and 1958). Energies are given for the corresponding configuration.

Table IV (continued)

(c) Intensity of peaks obtained in XPS using Al and $MgK\alpha$ x-rays. Intensities given relative to normal photoelectron peaks corresponding to photoionization in the outermost p shell.

(d) Quantum defect calculation of energy by Reader. (47)

18. A photoelectron spectrum of the valence shells of CsCl is shown in Figure 19.

An Al anode (1486.6 eV) and a Mg anode (1253.6 eV) were used for most of the runs. This made it possible to eliminate the peaks due to Auger transitions. For the spectrum of the Ar3p, 3s the Zr M ζ x-ray with an energy of 151.4 eV was also used for irradiation. The relative photoionization cross section σ_p/σ_{3s} was found to be much lower for the low energy Zr M ζ x-ray (Figure 13) than for either the Al⁽¹⁰⁾ or MgK $\alpha_{1,2}$ x-rays, which agrees with the theoretical calculations made by Scofield.⁽⁴¹⁾ This enables one to determine to what final state the satellite lines can be attributed. If the intensity of the satellite peaks follows that of the Ar3p then those peaks are a result of monopole transitions. If the intensity of the satellite lines remains the same relative to the Ar3p, then the satellite lines can be attributed to configuration-interaction.

Using the Zr 151.4 eV characteristic x-ray for irradiation, the intensity of the satellite line C shown in Figure 12 decreased as that of the Ar3s did. This implies that line C is due to configuration-interaction and not to monopole excitation of the Ar3p. Referring to Table III it is seen that the experimental binding energy of C is in excellent agreement with the configuration-interaction level $3s^2 3p^4 3d^2 S_{1/2}$ listed in the optical data.

When the MgK $\alpha_{1,2}$ 1253.6 eV x-ray were used for studying the outer shells of Ar the intensity of line C (cf. Figure 12) was much more than that of the satellite peak S. for the ZrM ζ x-ray (151.4 eV) the intensities of C and S (cf. Figures 13 and 14) became approximately the same.

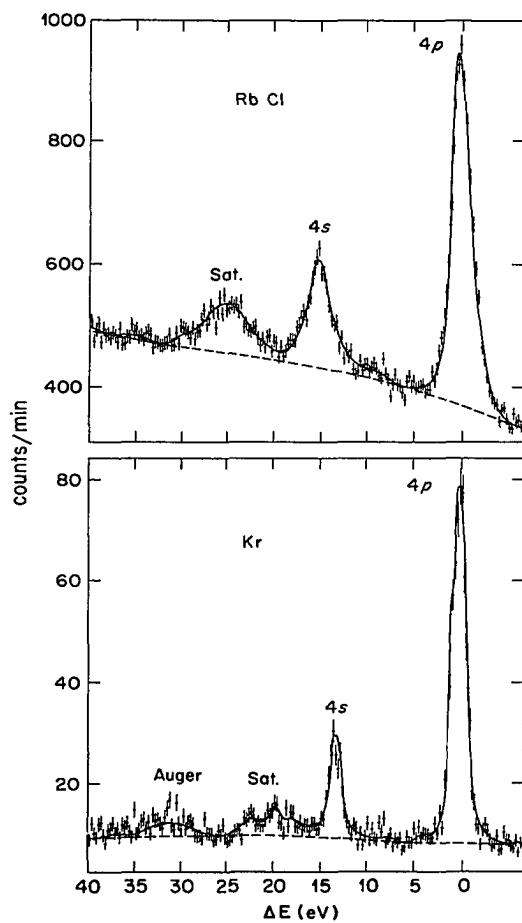


Figure 18. Photoelectron spectra of outer shells of Kr and Rb^+ in RbCl and their associated satellite lines using $M_gK\alpha$ x-rays.

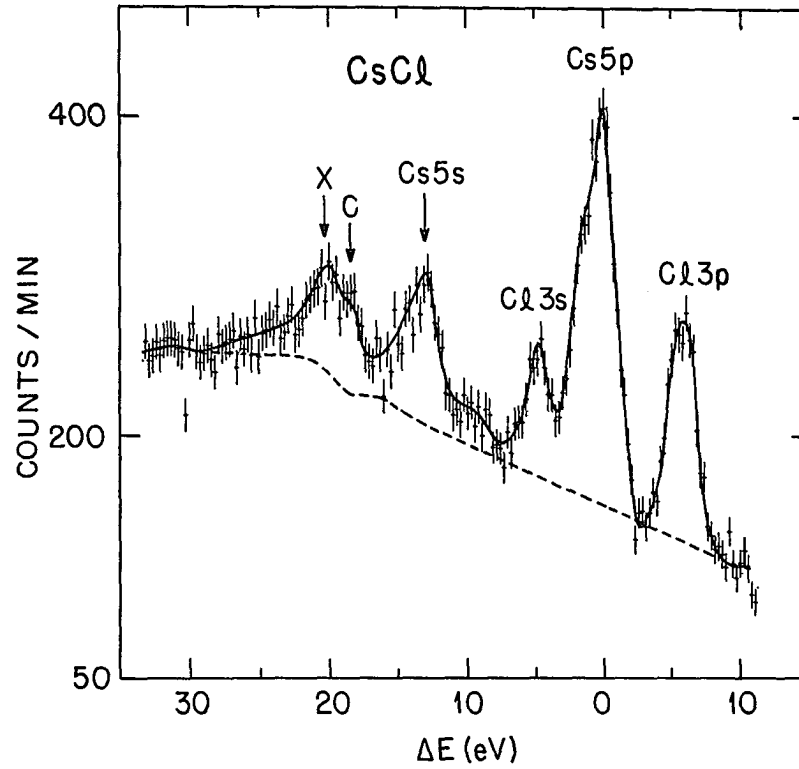


Figure 19. Photoelectron spectrum of valence shells of CsCl showing satellite structure associated with the Cs5s using MgK_{α} x-rays.

It was found that the intensity of S relative to that of the Ar3p remained about the same as when the Mg 1253.6 eV or Al 1483.6 eV x-rays were used. Peak S then is due to monopole excitation and the experimental binding energy corresponds very well with that calculated⁽¹⁸⁾ for the $3s^2 3p^4 4p \ ^2P^0$. This state for ArII corresponds to the similar level $2s^2 2p^4 3p \ ^2P^0$ of NeII which Carlson *et al*⁽¹²⁾ and Wuilleumier and Krause⁽¹⁴⁾ found to be one of the main monopole excited states seen in the spectrum of the outer shell of Ne.

The intensity of the peak labeled C' in Figure 13 followed the Ar3s intensity. This implies that this satellite line is due to configuration-interaction. The measured energy agrees very well with the energy calculated using the optical data⁽¹⁸⁾ for a $3s^2 3p^4 4d \ ^2S_{1/2}$ level.

Minnhagen,⁽⁴²⁾ in studying the optical spectrum of singly ionized argon, noted several anomalous energy shifts. He believed that these shifts were a result of configuration-interaction. He attributed the peaks to the mixing of the $Ar3s3p^5 \ ^2S_{1/2}$ with the $Ar3s^2 3p^4 4s \ ^2S_{1/2}$. Kj llerstr m⁽⁴³⁾ calculated the energy shifts for the electrostatic interaction between $3s3p^5 \ ^2S_{1/2}$ and $3s^2 3p^4 3d \ ^2S_{1/2}$, $3s^2 3p^4 4s \ ^2S_{1/2}$ in ArII, using wave functions based on the Thomas-Fermi-Dirac model of the atom. Their calculations show that both the interactions, $3s3p^5 \ ^2S_{1/2}$ and $3s^2 3p^4 3d \ ^2S_{1/2}$, $3s^2 3p^4 4s \ ^2S_{1/2}$ were possible. However, there was no indication of any contribution to the satellite structure in the photoelectron spectrum of Ar due to configuration mixing of the $3s 3p^5 \ ^2S_{1/2}$ and $3s^2 3p^4 4s \ ^2S_{1/2}$. If there is a 4s contribution it should have a binding energy 7.25 eV higher than the Ar3s. As Figure 12 shows, we were not able to observe such a line, at least not with

the present instrument. Also, there was no line noted at this energy by Carlson et al⁽¹⁰⁾ using the $\text{AlK}\alpha_{1,2}$ x-rays for excitation.

Cooper and Lavilla⁽⁴⁴⁾ observed a satellite peak in the $L_{2,3}$ x-ray emission spectrum of Ar. They tentatively assigned the satellite structure seen in their spectrum to mixing of the $3s3p^6\ ^2S_{1/2}$ with the $3s^23p^43d\ ^2S_{1/2}$, $3s^23p^44d\ ^2S_{1/2}$. This was later confirmed by Werme et al⁽⁴⁵⁾ using an x-ray grating spectrometer which had much better resolution than Cooper's and Lavilla's instrument.

We shall now consider the satellite lines in the x-ray photoelectron spectra of the outer shells of krypton shown in Figure 15. The analysis of the satellite structure is given in Table III. Observations made on argon have shown that the mixing of the $3s^23p^43d\ ^2S_{1/2}$ with the $3s3p^6\ ^2S_{1/2}$ to be the most important interaction. One would expect similar results with regard to krypton, i.e. mixing of the $4s4p^5\ ^2S_{1/2}$ and $4s^23p^44d\ ^2S_{1/2}$ configurations. Comparing the separation of the main satellite line from the $\text{Kr}4s$ the energy is found to be in excellent agreement with the optical data of Minnhagen et al⁽¹⁹⁾ for mixing of the $4s4p^5\ ^2S_{1/2}$, $4s^24p^44d\ ^2S_{1/2}$ configurations.

There is a small satellite line designated S with a slightly lower binding energy than the main satellite peak associated with the spectra of the outer shells of krypton. This could be the result of a monopole transition to the $4s^24p^45p\ ^2P^0$. The experimentally observed energy is in good agreement with the energy calculated.⁽¹⁸⁾ This monopole excited state also corresponds to the shake-up transition $3s^23p^5\ ^2P^0 \rightarrow 3s^23p^44p\ ^2P^0$ that was found to be of some importance in the case of argon.

It should be mentioned that this energy also corresponds closely to the $1a_1$ molecular orbital of H_2O . However, if there had been any moist air contamination the σ_u 2s of N_2 should be more intense than the $1a_1$ and this is not observed in the Kr 4p,4s photoelectron spectrum.

The interaction of the level $4s4p^6 \ ^2S_{1/2}$ and $4s^24p^45s \ ^2S_{1/2}$ may contribute some to the satellite intensity but the binding energy of the $4s^24p^45s \ ^2S_{1/2}$ appears to be too low to account for the peak labelled S. The broad peak approximately 18 eV from the Kr4s disappeared when an aluminum anode was used instead of a magnesium anode which would imply that it is due to an Auger transition.

There are several LMM Auger lines of krypton whose kinetic energies are such that they appear in the Kr4s spectrum when either the $MgK\alpha_{1,2}$ or the $AlK\alpha_{1,2}$ x-rays are used for irradiation. The main satellite line however, is not altered by changing the photon energy. One of the strongest LMM Auger lines of krypton⁽¹³⁾ has about the same kinetic energy as the $AlK\alpha$ induced Kr4s line. This makes it difficult to estimate the relative intensity of the satellite structure using an aluminum anode.

There are indications of two small peaks located at 8.9 eV and 10.6 eV. However, this energy range corresponds very closely to the LMM Auger line number 24 (K.E. = 1216.9 eV) listed by Siegbahn et al⁽¹³⁾ and is probably the cause of the peaks. There is also another LMM Auger line that makes it impossible to determine whether there is any real satellite structure in this region. A different photon energy must be used with a much more sensitive detector to completely answer the question.

In Figure 16 the spectrum of Xe5s and the main satellite lines associated with the outer shells is shown. The spectrum of Xe 5p,5s is shown in Figure 17 and an analysis is given in Table III. From the results on Ar and Kr one would expect that the most intense satellite line 5.6 eV from the Xe5s to be a result of the mixing of the level $5s5p^6 \ ^2S_{1/2}$ and $5s^25p^45d \ ^2S_{1/2}$. However the 5d state is on the low binding energy side of the main satellite line and cannot be responsible. The main satellite is probably due to configuration-interaction and is most likely to be a $5s^25p^4 \ nd \ ^2S_{1/2}$ level that can mix with the $5s5p^6 \ ^2S_{1/2}$. There is a configuration that Moore⁽¹⁸⁾ lists as a miscellaneous level 5.66 eV from the Xe5s photoelectron peak, designated 18, J = 1/2, that is in excellent agreement with the energy of the main satellite line. However, it is impossible to say that this is the excited configuration that is responsible for the main satellite line observed in the Xe5s photoelectron spectrum. Codling and Madden⁽²⁰⁾ made a very thorough absorption spectra study of Xe but did not attempt to make any configuration assignments. They state that before the spectra can be completely analyzed it will be necessary to carry out thorough theoretical calculations.

The main satellite line is asymmetric, giving evidence of another peak on the low binding energy side of it. There are four possible assignments with the two most probable being from the level $5s^25p^45d \ ^2S_{1/2}$, which can interact with the $5s5p^6 \ ^2S_{1/2}$ or can be due to the monopole transition $5s^25p^46p \ ^2P^0$. A configuration-interaction level $5s^25p^46s \ ^2S_{1/2}$ and a monopole excited state $5s^25p^46p \ ^2P^0$ are possibilities for the low binding energy side of the main satellite. Either the levels C and S

or C' and S' might be eliminated from consideration with better resolution and count rate.

In Figure 17 there are two satellite peaks 32.8 eV and 37.2 eV from the $Xe5p_{3/2}$. The possible lines from N_2 , O_2 and H_2O were checked but do not have the proper energies to account for either of the peaks. Also, there are no Auger electrons with this kinetic energy. In Cairns' et al⁽⁴⁸⁾ study of multiple ionization processes following photon absorption they point out the fact that there is a high probability of double and triple ionization. One would then expect to see satellite lines in the XeIII energy region. There are no lines listed by Moore⁽¹⁸⁾ with the proper energies but the satellite lines located at 32.8 and 37.2 eV in Figure 17 are probably due to configuration-interaction.

Alkali Metals

The alkali metal ions Na^+ , K^+ , Rb^+ and Cs^+ are isoelectronic with the rare gases Ne, Ar, Kr and Xe. Because of this it would be of interest to compare the satellite structures observed in the photoelectron spectra. For example, the photoelectron spectra of Rb^+ and Kr are compared in Figure 18. In each case, except Na^+ , the intensity of the satellite structure is higher for the alkali metal ion. There was no satellite structure seen in the Na^+ outer shell photoelectron spectra and is probably due to the fact that the $2s^2 2p^4 2d^2$ 2S configuration is not allowed. Werthein and Rosencwaig⁽¹⁶⁾ were the first to point out the very intense satellite structure in the alkali metal salts and to attribute it to electron excitation involving configuration-interaction states. The relative intensities and energies of the normal and satellite lines

associated with photoelectron spectra of the outermost s and p shells of the alkali metal ions are listed in Table IV. The satellite structures, using the $MgK\alpha$ x-rays, are in reasonable agreement with the earlier data of Wertheim and Rosencwaig using $AlK\alpha$ x-rays. Also listed are the energies for the states corresponding to the free ion as obtained from the optical data.⁽¹⁸⁾

The study of Wertheim and Rosencwaig of the outer shell of K included both KCl and KBr. In retaking the spectra it was noted that in the case of KBr the $MgK\alpha_{5/6}$ induced Br3d overlapped the satellite structure associated with the K3s. Taking this into account the shapes of the K3s satellite structures for KCl and KBr were in better agreement.

In addition to the difference in satellite intensities of K and Ar, the main satellite lines are a result of mixing of different configurations. Wertheim and Rosencwaig attribute some of the satellite structure to the mixing of the levels $3s3p^6\ ^2S_{1/2}$ and $3s^23p^43d\ ^2S_{1/2}$, but we believe that the main contribution to the satellite structure is due to the interaction of the $3s3p^6\ ^2S_{1/2}$ and $3s^23p^44s\ ^2S_{1/2}$, which, as shown above, is not significant in the case of Ar.

Whereas the photoelectron spectra and the x-ray emission spectra⁽⁴⁴⁾ satellite lines are both a result of mixing of the same configurations and therefore support each other, there is an unexplained difference in the interpretation of the x-ray and photoelectron spectra of K^+ . Cooper and Lavilla⁽⁴⁴⁾ attribute the main part of potassium $L_{2,3}$ x-ray emission satellite structure to the mixing of the $3s^23p^43d\ ^2S_{1/2}$ and $3s3p^6\ ^2S_{1/2}$, and not to the $3s^23p^44s\ ^2S_{1/2}$ and $3s3p^6\ ^2S_{1/2}$ that Wertheim

and Rosencwaig believed to be the most important in the photoelectron spectra.

Next the satellite structure in the photoelectron spectrum of the outer p and s shells of Rb^+ is compared with that of Kr, in Figure 18. Although the satellite intensity of Rb^+ is higher than that of Kr the main contribution to the satellite structure is due to the configuration mixing of the levels $4s4p^5 \ ^2S_{1/2}$ and $4s^24p^44d \ ^2S_{1/2}$. Wertheim and Rosencwaig have attributed the satellite structure in the photoelectron spectra of the outer s shell of Rb^+ to the mixing of the $4s4p^5 \ ^2S_{1/2}$ and $4s^24p^45s \ ^2S_{1/2}$, and to a less extent the $4s^24p^44d \ ^2S_{1/2}$. However, they were not aware of the work by Reader and Epstein⁽⁴⁶⁾ who studied RbIII in the free state and made corrections to the listed energies for several different levels of doubly ionized Rb. Two of the corrected levels were the $4s4p^5 \ ^2S_{1/2}$ and the $4s^24p^45s \ ^2S_{1/2}$. They also found the energy of the $4s^24p^44d \ ^2S_{1/2}$, which had not been listed before. With the corrections and new findings of Reader and Epstein,⁽⁴⁶⁾ Reader⁽⁴⁷⁾ was able to show the excellent agreement of the $4s^24p^44d \ ^2S_{1/2}$ with the energy of the main satellite line in the Rb4s spectrum. Reader indicates that the intensity of the 5s is approximately 1/3 that of the 4d with a small contribution from the 5d. He also states that a theoretical analysis of RbIII indicates that the level $4s4p^5 \ ^2S_{1/2}$ does interact strongly with the $4s^24p^44d \ ^2S_{1/2}$ and weakly with the $4s^24p^45s \ ^2S_{1/2}$.

In the case of CsCl it is impossible to say how much higher the relative satellite intensity is for Cs^+ than for Xe because of possible H_2O and O_2 contamination of the CsCl. The CsCl was loaded in an argon atmosphere but the sample may have already been contaminated. The spectrum

was run with every possible precaution taken to prevent any additional contamination. Then the sample was exposed to the air for almost an hour and the spectrum was taken again. The peak labelled X in Figure 19 increased in intensity and was assumed to be due to contamination. There was an overlap of this peak and satellite line which made the calculated relative satellite intensity very uncertain. There is no optical data available on CsIII but it is believed, based on this and other recent studies, that the main satellite line, which is 6.4 eV from the Cs5s is a result of configuration-interaction. In all cases the relative intensities of the satellite lines are much more for the alkali halides than for the rare gases. This is in disagreement with expectation from an atomic viewpoint. The total shake-up, shake-off probabilities for Ar and Ar⁺ were compared with the total shake-up, shake-off probabilities of K⁺ and K⁺⁺ using Hartree-Fock wave functions⁽²⁷⁾ and the total calculated probabilities were higher for Ar and Ar⁺. It is believed that the difference between the salts and the rare gases to be a solid state effect. Perhaps the d electrons in the conduction band in an alkali metal halide may have a greater overlap with the s and p core subshells than the corresponding overlap of the s, p and d orbitals in a free gas atom.

CHAPTER V

SATELLITE STRUCTURE IN MOLECULES

The photoelectron spectra of the core electrons of NO, N₂O, and H₂O, using MgK α x-rays as the photon source, are shown in Figures 20 through 23. An analysis of the spectra of the above molecules is given in Tables V, VI and VII. The photoelectron spectrum of the valence electrons of nitrogen is shown in Figure 5. In the case of N₂ the excitation source was the Zr M ζ 151.4 eV x-ray.

Photoionization in Core Shells

There have been several previous studies of shake-up peaks associated with core vacancies for diatomic and triatomic molecules.^(10,13,17,50) In all cases the sudden approximation is used to interpret the data. As with the rare gases the sudden approximation applied to molecules only allows for transitions described by monopole selection rules. These selection rules are

$$\Delta J = \Delta L = \Delta S = \Delta M = \Delta \Lambda = \Delta \Omega = \Delta \Sigma = 0 \quad .$$

For example for a $^1\Sigma_g^+$ state only a transition to another $^1\Sigma_g^+$ is allowed. However, Aarons et al⁽²⁸⁾ have pointed out that if the hole is localized then the u-g transitions become allowed. This analysis has been based on the localized hole concept, which is the assumption that a specific atom of a molecule has been ionized and the motion

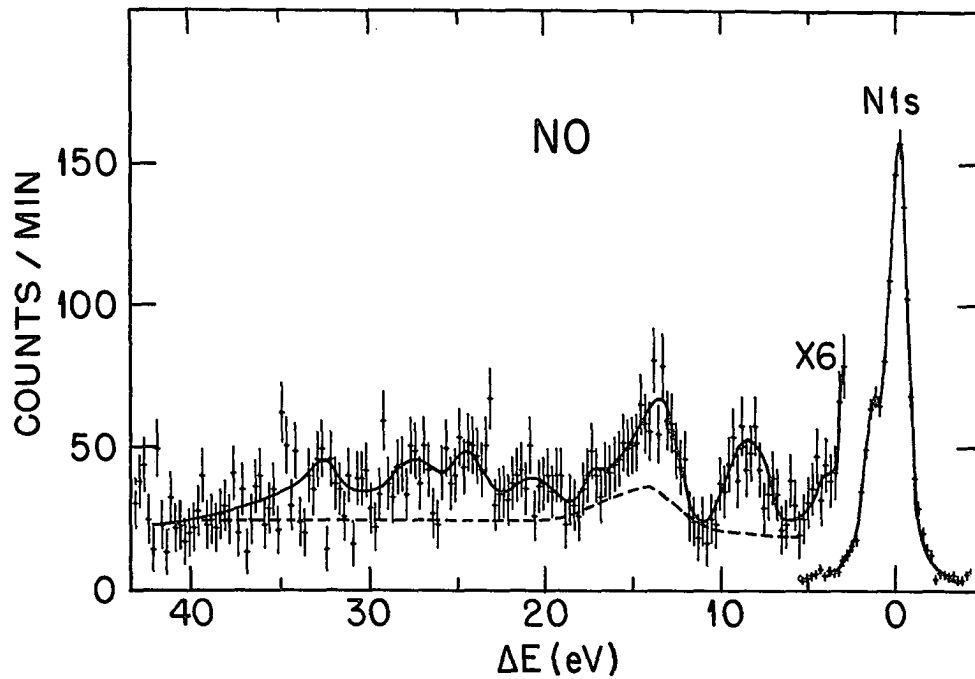


Figure 20. N1s photoelectron spectrum of nitric oxide and associated satellite structure using $MgK\alpha$ x-rays.

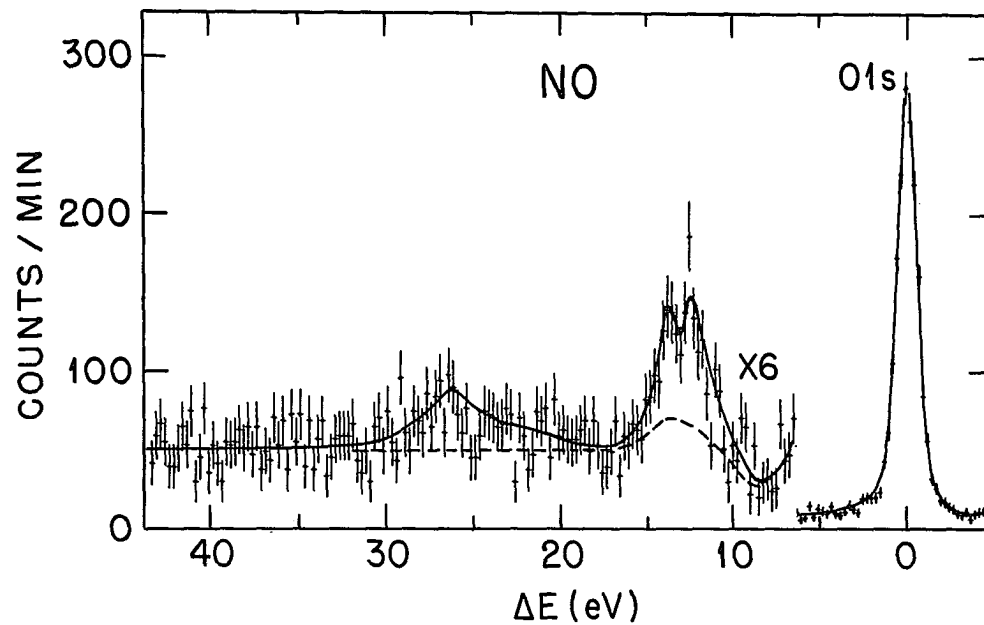


Figure 21. O1s photoelectron spectrum of nitric oxide and associated satellite structure using $MgK\alpha$ x-rays.

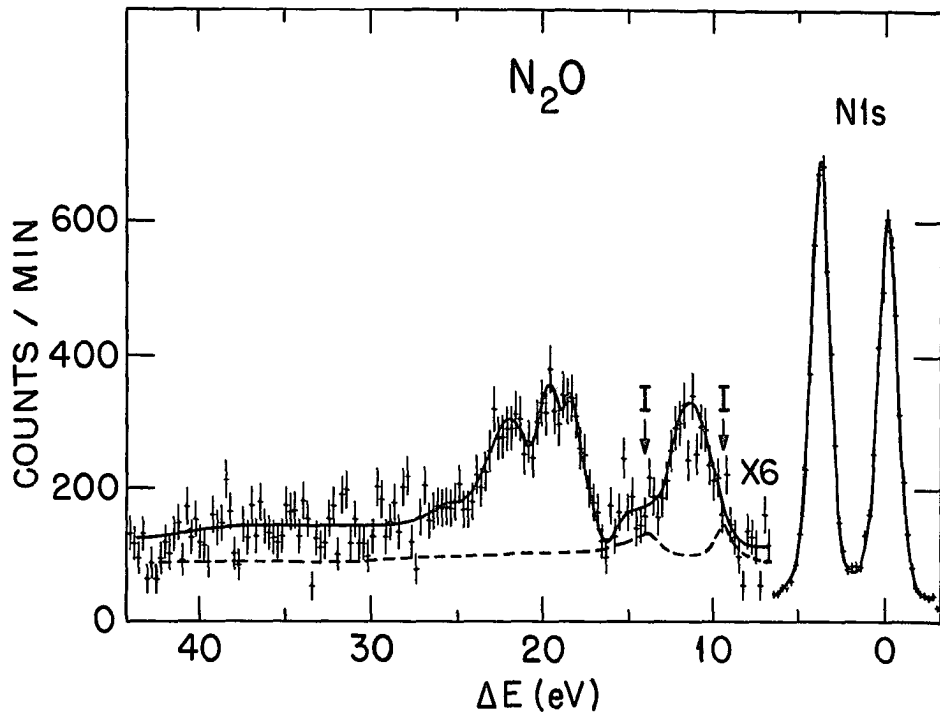


Figure 22. N_{1s} photoelectron spectrum of nitrous oxide and associated satellite structure using M_gK_α x-rays.

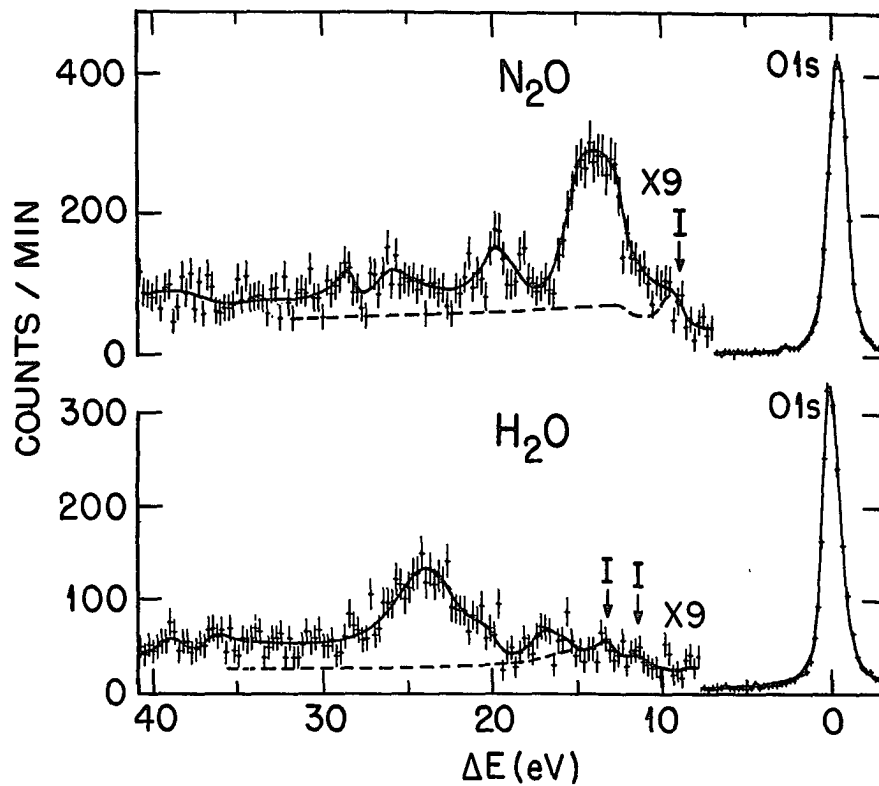


Figure 23. O1s photoelectron spectra of nitrous oxide and water showing their respective satellite structure using $M_gK\alpha$ x-rays.

Table V

Analysis of Satellite Structure in the Photoelectron Spectra of the Inner Orbitals of Nitric Oxide

Line	Exp Energy (ev) \pm 0.3	Intensity	Monopole Transitions	
			Neutral (NO)	Isoelectronic (O_2^+)
O1s	0	100		
s	12.5	7.0 \pm 2	$X^2 \rightarrow B^2 \sim 8 \text{ eV}^{(b)}$	
s	13.8	5.6 \pm 2	$X^2 \rightarrow B^2 \sim 6.5 \text{ eV}^{(b)}$	
s	26.7	3.8 \pm 1	$X^2 \rightarrow H^2 \sim 7 \text{ eV}^{(b)}$	
Total intensity		26	$X^2 \rightarrow K^2 \sim 8 \text{ eV}^{(b)}$	
			$X^2 \rightarrow L^2 \sim 9.96 \text{ eV}^{(d)}$	
N1s	0	100		
s	4.3	~ 2	$X^2 \rightarrow 2\pi \rightarrow 3\pi C_1^2 \sim 6.49 \text{ eV}^{(c)}$	$X^2 \rightarrow A^2 \sim 8 \text{ eV}^{(b)}$
s	8.5	5.5 \pm 2	$X^2 \rightarrow 2\pi \rightarrow 4\pi K^2 \sim 7.97 \text{ eV}^{(c)}$	$X^2 \rightarrow u \sim 11.9 \text{ eV}^{(a)}$
s	13.5	5.6 \pm 2	$X^2 \rightarrow 2\pi \rightarrow 5\pi Q^2 \sim 8.51 \text{ eV}^{(c)}$	
Total intensity		26		
			$1\pi \rightarrow n\pi \sim 12 \rightarrow 17 \text{ eV}^{(c)}$	
			$X^2 \rightarrow P^2 \sim 18.8 \text{ eV}^{(d)}$	

(a) From vertical transition energy given by Edqvist *et al.* (52)

(b) Estimated energies of Franck-Condon transitions using energy curves by Gilmore. (54)

(c) From Rydberg series calculated by Edqvist *et al.* (58)

(d) From energies of electronic states of nitric oxide calculated by Lefebvre-Brion and Moser. (59)

Table VI
 Analysis of Satellite Structure in the Photoelectron Spectra of the
 Inner Orbitals of Nitrous Oxide

Line	Exp. Energy (eV) \pm 0.3	Relative Intensity	Neutral Molecule (N ₂ O)	Isoelectronic (NO ₂ ⁺)
01s	0	100		
s	14.3			
s	20.0			
Total intensity		~ 24%		
N1s #1	0	100	X $1\Sigma^+ \rightarrow 21\Sigma^+$ 13.6 eV ^(a)	$6a_1^{-1} 1A_1 \rightarrow 5a_1^{-1} 1A_1$ 10 eV ^(b)
N1s #2	4.3	-		
s	11.5	-		
s	18.	-		
s	19.7	-		
s	21.7	-		
s	22.5	-		
Total intensity		~ 25%		

(a) See reference (56).

(b) See reference (66).

Table VII
 Analysis of Satellite Structure in the Photoelectron Spectra
 of the Inner Orbitals of Water

Line	Exp. Energy (eV) \pm 0.3	Relative Intensity	Neutral Molecule (H ₂ O)
O1s	0	100	$\bar{X}^1A_1 \rightarrow \bar{B}^1A_1$ 8.8 eV ^(a)
s	23.7	\sim 14	$\bar{X}^1A_2 \rightarrow D^1A_1$ 12.0 eV ^(a)

(a) See reference (64).

of the valence electrons is correlated with the location of the core hole. This is possible if the valence electrons of a molecule can relax toward the core hole in a time that is small compared to the time for exchange between equivalent core sites. Also the localized hole concept has been shown by Snyder⁽⁵¹⁾ and Bagus and Schaefer⁽⁴⁰⁾ to be correct in their theoretical calculations. Herzberg⁽⁶⁵⁾ also states that the u,g symmetry loses its importance when considering molecules made up of different atoms.

One would like to make configuration assignments on the observed satellite lines. However, it is difficult to make any assignments because there is no optical data available and there are no known theoretical calculations for core shell ionization for the molecules studied in this work. A neutral molecule that is isoelectronic with an ion is expected to have similar molecular structure and molecular orbitals. For example CO and N₂ are isoelectronic with NO⁺. One might then expect to be able to compare the separation of the satellite line from the normal photoelectron peak with the energies of monopole excited levels. This method has been used by Carlson et al⁽¹⁰⁾ in their study of CO and N₂.

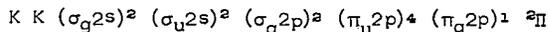
A second procedure has been used to try to interpret satellite structure in the photoelectron spectra of molecules. The energy separation of the shake-up lines can be compared with monopole excited levels of the neutral molecule. It is assumed that the perturbation following a core shell ionization is independent of the energy levels and the occupied and unoccupied molecular orbitals of the neutral molecule will relax by the same amount. Allan et al⁽¹⁷⁾ have used this approach

to make assignments to the shake-up peaks seen in the inner orbital spectra of CO_2 , COS and CS_2 . Both of the above described methods will be used in an attempt to interpret the satellite structure seen in the photoelectron spectra of the molecules.

When the potential energy curves of the neutral molecules and ions are available the energy given for the monopole excitation can be estimated for a Franck-Condon transition. However, several of the energies are given only for the ground state of the excited levels and may be too low.

Nitric Oxide

The first molecule to be considered is nitric oxide. The ground state configuration of nitric oxide is



The molecule possesses a single unpaired electron. The spectra of both the N1s and O1s, which can be seen in Figures 20 and 21, were studied. An analysis of the spectra is given in Table V. Both the N1s and O1s spectra have satellites with a binding energy approximately 13 eV to 15 eV higher than the normal photoelectron peak. The N1s spectrum is very rich in satellite structure. In addition to the main satellite previously mentioned there is a small peak located 4.3 eV from the main N1s line and another 8.5 eV. There are also several satellite lines in the region from 16 eV to approximately 32 eV. In the case of the O1s spectrum the main satellite line is about 13 eV from the

O1s there is a small, broad peak located approximately 27 eV from the normal O1s.

As noted before the main satellite lines in both the N1s and O1s are about the same distance (13 to 15 eV) from the normal photoelectron peaks. The similarity in the energy separations indicates that the same molecular orbitals are involved in the monopole transition.⁽⁵⁰⁾

To determine the possible monopole excited states that might account for the shake-up peaks, the spectrum of NO is compared with the energies of the isoelectronic ion O_2^+ . The data listed by Edqvist,⁽⁵²⁾ Yoshino and Tanka⁽⁵³⁾ and the potential curves of Gilmore⁽⁵⁴⁾ are used to determine the energies of the different molecular orbitals. The energy levels of O_2^+ are listed with the ungerade, gerade symmetry being distinguished. Nitric oxide is made up of two different atoms and the u,g symmetry can be neglected. This would mean that of the levels that are listed only two monopole excited transitions are allowed from the ground state of $X^2\Pi_g$ of O_2^+ . They are (1) $X^2\Pi_g \xrightarrow{5 \text{ eV}} A^2\Pi_u$ (2) $X^2\Pi_g \xrightarrow{11.9 \text{ eV}} a^2\Pi_u$. The small satellite line located at 4.3 eV corresponds closely to the $X^2\Pi_g \rightarrow A^2\Pi_u$, where again the u,g symmetry property must be ignored. However, if the Franck-Condon principle is applied for the $X^2\Pi_g \rightarrow A^2\Pi_u$ transition, the energy separation, using the potential energy curves by Gilmore,⁽⁵⁴⁾ is about 8 eV which corresponds closely to the energy of the satellite line at 8.5 eV in the N1s spectrum. The excitation energies of the main satellite lines in both the N1s and O1s spectra are about the same as the monopole transition $X^2\Pi_g \xrightarrow{11.9 \text{ eV}} a^2\Pi_u$ listed by Edqvist et al.⁽⁵²⁾ Although this procedure does give a tentative explanation for two of the satellite lines, the

$X \ ^2\Pi_g \xrightarrow{11.9 \text{ eV}} \ ^2\Pi_u$ energy difference is lower than the separation seen in the photoelectron spectra.

A second procedure following Allan et al⁽¹⁷⁾ was used in an attempt to interpret the satellite lines seen in the N1s and O1s spectra of nitric oxide using the Rydberg series of Edqvist et al⁽⁵²⁾ and the potential energy curves of Gilmore.⁽⁵⁴⁾ Comparing the excited states of neutral nitric oxide listed in Table V there is seen to be several monopole transitions that might account for the satellite lines. The first satellite line for the first excited state is seen to be associated with the N1s photoelectron peak. There is no corresponding satellite line at 8.5 eV in the O1s spectrum. This indicates that the ground state molecular orbital involved in the excitation responsible for the line at 8.5 eV is localized on the nitrogen. The monopole transition from the ground state of neutral molecule $X \ ^2\Pi$ to the level $B \ ^2\Pi \sim 8 \text{ eV}$.⁽⁵⁴⁾ This is the monopole excited transition that is expected to be the most likely. However, there are several more monopole transitions listed in Table V that are in the correct energy range. These are transitions of the $\pi 2p$ molecular to monopole excited levels. One would expect the first excited transition to involve the $\pi 2p$ orbital and comparing the data with the energy of the levels taken from Gilmore's⁽⁵⁴⁾ energy curves and the Rydberg series of Edqvist et al⁽⁵⁸⁾ would tend to verify this. Brion et al⁽⁵⁷⁾ give the atomic populations for each atomic orbital on nitrogen and oxygen. In the case of $2p\pi$ orbital the population on the nitrogen is 65% and 35% on the oxygen atom. We have seen above that the satellite peak located at 8.5 eV in the N1s spectrum corresponds closely to the monopole excited states for

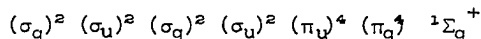
monopole transitions of the $2p\pi$ molecular orbital. Also, the atomic population calculations show that the $2p\pi$ molecular orbital is most likely to be found associated with the nitrogen atom. These two facts would tend to verify that the satellite peak located at 8.5 eV in the N1s spectrum is associated with the monopole transition of the $2p\pi$ molecular orbital.

Next the main satellite lines in the 13 eV to 15 eV range of both the N1s and O1s spectra are considered. As noted before, the fact that the energy range of the two satellite are similar indicates that they may be from the same ground state molecular orbital. The energy is too high to be due to a monopole excitation of the $2p\pi$ molecular orbital. The next molecular orbital is the 1π ⁽⁵⁸⁾ which is a combination of the $2p$ atomic orbital of nitrogen and the $2p$ atomic orbital of oxygen. The energies of the monopole excited states for the 1π molecular orbital (see Table V) are in the 12 to 17 eV range which corresponds to the position of the most intense satellite lines seen in both the N1s and O1s spectra. Brion and Yamazaki⁽⁵⁷⁾ give the atomic populations for the 1π molecular orbital. The values they list are ($2p\pi$ 1.42) for the nitrogen and ($2p\pi$ - 2.58) for the oxygen. The main satellite line in the O1s spectrum is more intense than the main satellite peak in the N1s spectrum. This qualitative intensity and energy agreement indicate that the monopole transition responsible for the main secondary peaks in the N1s and O1s spectra probably involve the 1π molecular orbital. The satellite lines further separated from the O1s and N1s must be due to monopole excitation from lower lying molecular orbitals. The N1s

and O1s spectrum show that the molecular orbitals involved probably have higher atomic population densities on the nitrogen atom.

Nitrous Oxide

Nitrous oxide is a linear triatomic molecule (N-N-O) with the two nitrogens in a different chemical environment. This is evident when the spectrum of the N1s is observed. The binding energy of the central nitrogen is 4.3 eV higher than the outer nitrogen. The ground state configuration is



The N1s and O1s spectra are shown in Figures 22 and 23, and an analysis of the spectra is given in Table VI.

In the case of the N1s spectrum there are two main contributions to the satellite structure. It is assumed that the first satellite line located at 11.5 eV in the N1s spectrum (Figure 22) is associated with photoionization in the 1s shell of the outer nitrogen. There is only a small contribution at this energy in the case of the O1s spectrum, and appears as a shoulder on the main satellite line in the O1s spectrum. The broad satellite structure centered at approximately 20 eV (Figure 22) is probably associated with both of the nitrogen atoms.

The O1s spectrum of N₂O has one main satellite 14.3 eV from the normal photoelectron peak and a small shake-up peak at 20 eV. There is a shake-up line located 14.4 eV from the center nitrogen N1s peak which is almost the same separation as that of the main shake-up peak in the O1s spectrum. This indicates that they may both involve the same

molecular orbitals. However, it is not completely clear that this would be true if a localized hole model is assumed.

In order to try to interpret the N_2O data and make some tentative assignments of the monopole transitions involved the energy separations of the shake-up peaks are compared with the excited levels of the isoelectronic ion NO_2^+ . The excited levels of NO_2^+ are taken from Edqvist *et al.* (66). The configuration are given for a molecule which belongs to the C_{2v} symmetry group. The ground state of NO_2^+ is $6a_1^{-1} 1A_1$ which means that for a monopole transition another $1A_1$ level must be found. There is only one $1A_1$ state listed by Edqvist *et al.* (66). This is the $5a_1^{-1} 1A_1$ where the energy difference for the $6a_1^{-1} 1A_1$ transition is approximately 10 eV. This energy is too low to account for any of the shake-up peaks seen in the N1s and O1s spectra.

Secondly the N_2O data is compared with the excited levels of the neutral molecule.

In the case of N_2O only a few of the energy levels with designations are listed. (64,55) However, Peyerimhoff and Buenker (56) have made configuration-interaction calculations to obtain the ground state energy and the energies of numerous excited states. There is only one monopole excited transition listed, $X^1\Sigma^+ \underline{13.6 \text{ eV}} 2^1\Sigma^+$ which corresponds in any way to an observed satellite peak. This is the shake-up line located 14.3 eV from the O1s of N_2O that might be due to the above mentioned shake-up transition.

Brion and Yamazaki (57) list several Rydberg series for nitrous oxide. Several of these are listed in Table VI but none of the energy differences involved are enough to account for any of the satellite lines.

The atomic population densities calculated by White* for N_2O was used in an attempt to make a qualitative interpretation of the N1s and O1s photoelectron spectra. One would expect the π_g molecular orbital to be involved in the first excited transition. The population densities given in Table VIII show that the π_g has a high probability of being associated with the end nitrogen and very low density at the center nitrogen. The intensity of the first satellite peak seen in the N1s spectrum follows the relative calculated density in the case of the two normal nitrogen peaks. There is the main peak at 11.5 eV associated with the center nitrogen (low binding energy). There is little if any satellite structure located at 15.8 eV that would be the corresponding shake-up peak for the 1s spectrum of the center nitrogen, which does agree with the atomic population calculations for the π_g molecular orbital. Also, the intensity of the first excited level in the N1s corresponds to the density one would expect from the calculated atomic densities for the π_g molecular orbitals. Although, the energy separation of the O1s satellite line, 14.3 eV, is more than the separation of the satellite peak of the first excited state, 11.5 eV, of the N1s the fact that one would have to consider a localized hole may account for the discrepancy in the separation. Theoretical calculations for a core hole vacancy on the oxygen and then on the nitrogen should clarify this point.

*These calculations were done by R. M. White of Baker University using a code acquired from the Quantum Chemistry Program Exchange (see Ref. 19).

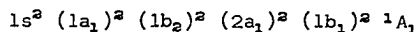
Table VIII
Atomic Contributions to Atomic Orbitals for N_2O^*

Orbital	N(center)	N(end)	O
π_g	1.2	31.6	67.2
σ_u	21.6	34.8	43.6
π_u	50.0	28.6	21.4
σ_g	12.7	53.7	33.5

*These calculations were done by R. M. White of Baker University using a code acquired from the Quantum Chemistry Program Exchange (see Ref. 19).

The second large satellite structure centered about 20 eV from the 1s peak of the end nitrogen may have contributions from both of the N1s peaks. The next lowest molecular orbital is the 2s2p. This level lies 3.5 eV⁽⁵⁵⁾ lower than the 2pπ_g. The observed separation of the first satellite peak located at 11.5 eV from the second satellite peak at about 19.2 eV is ~ 8 eV. This is more than the 3.5 eV one would expect the separation to be following core shell ionization. The contribution to the 2p2sσ molecular orbital from the end and center nitrogens given in Table VIII agrees qualitatively with the assumption that there should be a fairly intense structure from both nitrogens for excitation of the σ_u molecular orbital. In addition, there is a small satellite line in the O1s spectrum (Figure 23) located at 20.0 eV that corresponds to the satellite lines located about 19 eV from the N1s peaks.

Next water is studied and the spectrum of the O1s is shown in Figure 23. The analysis of the spectrum is given in Table II. In the ground state the H-O-H angle is 104.5° and the molecule to the C_{2v} point group. The H₂O ground state configuration is



The molecular orbital 1b₁ is the 2p_x atomic orbital of oxygen. Most of the shake-up contribution is contained in the peak located 23.7 eV from the O1s. The satellite intensity relative to the O1s is ~ 15%. Comparing the main satellite positions and total shake-up intensities of H₂O, 23.7 eV and ~15% to that of the O1s of N₂O, 14.3 eV and ~ 25% point out the fact that the satellite intensity and separation reflect somewhat the different environment of the oxygen atom.

H_2O is isoelectronic with H_2F^+ but very little is known⁽⁶¹⁾ about this ion and no comparison could be made.

Secondly, the neutral molecule is considered and the excited levels are found. Several excited levels of neutral H_2O are listed by Herzberg⁽⁶⁴⁾ and are given in Table VII. The two monopole allowed states for the neutral molecule are $\tilde{\text{B}}^1\text{A}_1$ and $\tilde{\text{D}}^1\text{A}_1$ which are respectively 8.8 eV and 10.2 eV above the ground state. The observed satellite line in the O1s spectrum of H_2O is located at 23.7 eV, which is more than twice the energy of the monopole excited levels that are listed. The fact that there was some success in using the levels of the neutral molecule N_2O as a guide line for interpreting the data in that case and not for H_2O may be due to the fact that removal of an O1s electron from H_2O caused a relatively larger perturbation to the water molecule than the removal of an electron in the case of nitrous oxide.

In both cases the attempt to interpret the data by comparing the energy separations with excited states of an isoelectronic ion and using the neutral molecule for comparison met with some success. The use of the Mulliken density calculations seemed to give some insight into the transitions involved. However, none of the approaches were able to account for all of the satellite lines seen. This clearly indicates the need for more molecular orbital calculations in order to determine the mechanism involved in forming the satellite lines in the molecular photoelectron spectra.

Photoelectron Spectra of Valence Shells

The final topic is a study of photoionization in the outer orbitals of N_2 . The spectrum has previously been run by Siegbahn et al.⁽¹³⁾ using the Mg K α x-ray for irradiation. The spectrum shown in Figure 24 was taken using the Zr M ζ 151.4 eV characteristic x-ray for excitation. The main difference noted in the two spectra was the large change in relative intensity of the photoelectron lines. This can be seen in Table IX where the intensity of the molecular orbitals for Zr and Mg is compared to the $\sigma_u 2s$. The $\pi_u 2p$ and the $\sigma_g 2p$ intensities increase while the $\sigma_u 2s$ decreases. The peak labeled A, 21.5 eV from the $\pi_u 2p$, also has a very large increase in intensity while the $\sigma_g 2s$ becomes the dominant peak. This indicates that A has a strong 2p dependence. This may indicate that peak A is a result of monopole excitation of the $2p\pi_u$ and $2p\sigma_g$ molecular orbitals. The spectrum of Siegbahn et al.⁽¹³⁾ and Gelius⁽⁵⁰⁾ show a small satellite peak that should be located at 8.2 eV in the N_2 valence shell photoelectron spectra. Siegbahn et al⁽¹³⁾ attributes this to the configuration mixing of the $B^2\Sigma_u^+$ and $C^2\Sigma_u^+$. This satellite is not visible in the N_2 spectrum shown in Figure 5. This would be consistent with the intensity decrease of the $\sigma_u 2s$ and would imply that Siegbahn's et al⁽¹³⁾ assumption was correct.

The satellite structure located in the 10 to 15 eV range, Figure 24, of the N_2 spectrum is too intense to be totally due to inelastic collision peaks. Gelius⁽⁵⁰⁾ reports on the photoelectron spectrum of the N_2 outer orbitals using a very high intensity, high resolution instrument, and observes several satellite peaks with binding energies from

Table IX
Analysis of Valence Shell Photoelectron Spectra of N₂

	Line	XPS eV ± 0.3	Binding Energy (eV) ^(e)	Optical Data	Intensities	
					A ₂ ^(d)	Zr
X ² Σ _g ⁺	σ _g 2p	- 1.3	15.5	15.576 ^(c)	~ 15	~ 75
A ² u	π _u 2p	0	16.8	16.9 ^(b)	~ 5	~ 85
B ² u ⁺	σ _u 2s	1.8	18.6	18.733 ^(c)	100	100
C ² Σ _u ⁺	σ _u 2s ^(a)	8.2	25.0	25.3 ^(b)	-	-
² Σ _g ⁺	σ _g 2s	19.0	37.3		~165	~340
	A	23.0	--	--	~ 17	~ 54

(a) Listed by Siegbahn to be due to configuration mixing with σ_u2s (cf. ref. 13).

(b) Gilmore (cf. ref. 54).

(c) Herzberg (cf. ref. 65).

(d) The spectrum shown in Gelius' thesis was used in the case of the aluminum anode.

(e) Seigbahn (cf. ref. 13).

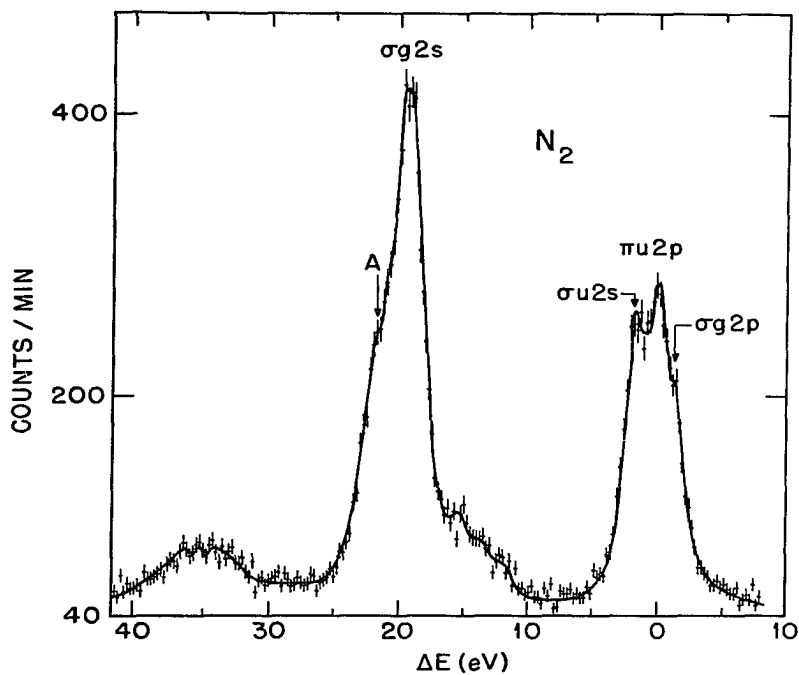


Figure 24. Photoelectron spectrum of valence shells of N_2 using ZrM_6 x-rays.

22.5 eV to approximately 32 eV. The N_2 pressure was low enough to rule out the possibility of inelastic collision peaks. In observing our spectrum it is impossible to tell if the intensity of the satellite lines located in the 10 to 15 eV range has increased along with the intensities of $\sigma_g 2p$ and $\pi_u 2p$. Most of the satellite structure centered at approximately 35 eV is due to inelastic collisions but it does seem a little high to be totally accounted for by inelastic collisions.

Summary

The excitation following photoionization in the core shells of the rare gases fell within the framework of the sudden approximation. The satellite intensities and energies were for the most part independent of the core vacancy. Also, there was seen to be no strong dependence on the photon energy used for excitation.

When photoionization occurs in the valence shells of argon, krypton, and xenon the satellite lines are due mainly to configuration interaction. The proper configuration assignments were made in the case of argon and for the main satellite line observed in the krypton valence shell photoelectron spectrum using the optical data. No assignments were made in the case of xenon. Similar satellite structure was seen in the valence shell photoelectron spectra of the isoelectronic alkali metal ions but with larger relative intensities than those of the rare gases.

There was observed excitation following photoionization in the core shells of nitric oxide, nitrous oxide and water. In the case of nitric oxide and nitrous oxide there was some success in interpreting the satellite structure by comparing the separations from the normal

photoelectron peak with the monopole excited levels of the neutral molecule and an isoelectronic molecule. Also, using Mulliken density calculations added some insight into the possible excitation processes. In the case of water there was no information available on the isoelectronic molecule H_2F^+ . The satellite separation from the normal photoelectron line is more than twice the separation that the monopole excited levels of neutral H_2O would indicate.

In the case of N_2 there was observed to be a strong energy dependence of the photoionization cross sections of the valence shell molecular orbitals. Using the ZrMg x-ray for excitation instead of the $\text{AlK}\alpha$ and $\text{MgK}\alpha$ x-rays increased the intensities of the satellite line observed on the high binding side of the σ_g2s , the π_u2p and the σ_g2p .

LIST OF REFERENCES

LIST OF REFERENCES

1. P. D. Innes, Proc. Roy. Soc., A IXXIX, 442 (1907).
2. H. Robinson and W. F. Rawlinson, Phil. Mag., 28, 277 (1914).
3. Ralph G. Steinhardt and Earl J. Serfass, Anal. Chem., 23, 1585 (1951).
4. K. Siegbahn and K. Edvarson, Nuc. Phys., 1, 137 (1956).
5. R. Sokolowski, C. Nordling and K. Siegbahn, Arkiv Fysik, 12, 301 (1957).
6. H. G. Kuhn, Atomic Spectra, Longmans, Green and Co. Ltd., 1962, Ch. V.
7. David Bohm, Quantum Theory, Prentice-Hall Inc., 1951, p. 507.
8. T. A. Carlson, Phys. Rev., 156, 142 (1967).
9. J. A. R. Samson, Phys. Rev. Lett., 22, 693 (1969).
10. T. A. Carlson, M. O. Krause and W. E. Moddeman, J. de Physique, 32, C4-76 (1971).
11. M. O. Krause and F. Wuilleumier, J. Phys. B: Atom Molec. Phys., 5, L143 (1972).
12. M. O. Krause, T. A. Carlson and R. D. Dismukes, Phys. Rev., 170, 37 (1968).
13. K. Siegbahn, C. Nordling, G. Johansson, J. Hedman, P. F. Heden, K. Harmin, U. Gelius, T. Bergmark, L. O. Werme, R. Manne and Y. Baer, ESCA Applied to Free Molecules, North-Holland Pub. Co., 1969.
14. F. Wuilleumier and M. O. Krause (to be published).
15. U. Gelius, E. Basilier, S. Svensson, T. Bergmark and K. Siegbahn, Univ. of Uppsala Report, UUIP-817.

16. G. W. Wertheim and A. Rosencwaig, Phys. Rev. Lett., 26, 1179 (1971).
17. C. J. Allan, U. Gelius, D. A. Allison, G. Johansson, H. Siegbahn and K. Siegbahn, J. Elect. Spect., 1, 131 (1972).
18. C. E. Moore, Atomic Energy Levels, Vols. I, II, and III, NBS 467, U. S. Govt. Printing Office, Washington, D. C., 1949, 1952, and 1958.
19. L. Minnhagen, H. Strihed and B. Petersson, Arkiv För Fysik, 39, 471 (1969).
20. K. Godling and R. P. Madden, J. of Research, 76A, 1 (1972).
21. F. W. Byron, Jr. and C. J. Joachaim, Phys. Lett., 24A, 616 (1967).
22. B. P. Pullen, T. A. Carlson, W. E. Moddeman, G. K. Sweitzer, W. E. Bull and F. A. Grimm, J. of Chem. Phys., 53, 768 (1970).
23. T. A. Carlson (to be published).
24. F. Block, Phys. Rev., 48, 187 (1935).
25. J. S. Levinger, Phys. Rev., 90, 11 (1953).
26. T. A. Carlson, C. W. Nestor, Jr., T. C. Tucker and F. B. Malik, Phys. Rev., 169, 27 (1968).
27. T. A. Carlson and C. W. Nestor, Jr. (submitted to Phys. Rev.).
28. L. J. Aarons, M. F. Guest and I. H. Hillier, J. Chem. Soc., Trans. Faraday Soc., II, 68, 1866 (1972).
29. U. Fano and J. W. Cooper, Rev. Mod. Phys., 40, 441 (1968).
30. D. R. Hartree, Proc. Cambridge Phil. Soc., 24, 111 (1928).
31. V. Fock, Zeit. F. Phys., 126 (1930).
32. Hendrik F. Hameka, Introduction to Quantum Theory, Harper and Row, New York, 1967.

33. Charles S. Fadley, Lecture Notes for the NATO Advanced Study Institute on "Electron Emission Spectroscopy," Gent University, Gent, Belgium, August 1972.
34. John C. Slater, Quantum Theory of Atomic Structure, Vol. II, McGraw-Hill Book Co., Inc., 1960.
35. Charlotte Froese Fischer, Comp. Phys. Comm., 1, 151 (1969).
36. M. O. Krause and O. Keski-Rahkonen (to be published).
37. E. E. Salpeter and M. H. Zaidi, Phys. Rev., 125, 24B (1962).
38. Robert L. Brown, Phys. Rev. A, 1, 341 (1970).
39. Teijo Aberg, Asymptotic Double Photoexcitation Cross Sections of the Helium Atom, Laboratory of Physics, Technical University of Helsinki, Otaniemi, Finland, Research Report 2, 1970.
40. Paul S. Bagus and Henry F. Schaefer III, J. Chem. Phys., 56, 224 (1972).
41. J. H. Scofield, Theoretical Photoionization Cross Sections from 1 to 1500 keV, Univ. of Calif. Radiation Lab. Rpt. UCRL 51326, 1973.
42. L. Minnhagen, Ark. Fys., 25, 203 (1963).
43. B. Kjällerström, N. H. Möller and H. Svensson, Arkiv Föer Fysik, 29, 167 (1965).
44. J. W. Cooper and R. E. Lavilla, Phys. Rev. Lett., 25, 1745 (1970).
45. L. O. Werme, B. Grennberg, J. Nordgren, C. Nordling and K. Siegbahn, Phys. Letters A, 41, 113 (1972).
46. J. Reader and G. L. Epstein, J. Opt. Soc. Am., 62, 1467 (1972).
47. Joseph Reader, Phys. Rev. A, 7, 1431 (1973).
48. R. B. Cairns, H. Harrison and R. I. Schoen, Phil. Trans. Roy. Soc. Lond. A, 268, 163 (1970).

49. E. Lindholm, Arkiv För Fysik, 40, 97, 103, 125 (1969).
50. U. Gelius, Electron Spectroscopy, Proceedings of Conference held in Asilomar, Calif., Sept. 1971, ed. D. A. Shirley (North-Holland Pub. Co., Amsterdam, 1972), p. 311.
51. L. C. Snyder, J. Chem. Phys., 55, 95 (1971).
52. O. Edqvist, E. Lindholm, L. E. Selin and L. Asbrink, Physica Scripta, 1, 25 (1970).
53. K. Yoshino and Y. Tanaka, J. Chem. Phys., 48, 4859 (1968).
54. Forrest R. Gilmore, J. Quant. Spect. Rad. Trans., 5, 369 (1965).
55. D. W. Turner, C. Baker, A. D. Baker and C. R. Brundle, Molecular Photoelectron Spectroscopy, Wiley, New York, 1970.
56. S. D. Peyerimoff and Robert J. Buenker, J. Chem. Phys., 49, 2473 (1968).
57. H. Brion, C. Moser and M. Yamazaki, J. Chem. Phys. 30, 673 (1959).
58. O. Edqvist, E. Lindholm, L. E. Selin, H. Sjogren and L. Asbrink, Arkiv För Fysik, 40, 439 (1969).
59. H. Lefebvre-Brion and C. M. Moser, J. Chem. Phys., 44, 2951 (1966).
60. T. A. Carlson and A. E. Jonas, J. Chem. Phys. 55, 4913 (1971).
61. Michel Couzi, Jean-Claude Cornut, and Pham Van Huong, J. Chem. Phys., 56, 426 (1972).
62. T. A. Carlson and M. O. Krause, Phys. Rev., 140, A1057 (1965).
63. E. U. Condon and G. H. Shortley, The Theory of Atomic Spectra, University Press, Cambridge, England, 1967.
64. G. Herzberg, Electronic Structure of Polyatomic Molecules, D. Van Nostrand Co., Inc, 1967.

65. G. Herzberg, *Molecular Structure and Molecular Spectra, Vol. I Diatomic Molecules*, D. Van Nostrand Co., Inc., 1967.
66. O. Edqvist, E. Lindholm, L. E. Selin and L. Åsbrink, *Physica Scripta*, 1, 172 (1970).